3. 感覚提示実験

感覚神経への電気刺激によって生成される圧感覚の強度はパルス頻度に依存している [3] 事が報告されており，本研究ではこの関係を応用する．

3.1 実験目的・方法

本実験の被験者は，健全な男性 1 名である．被験者は座っており，開眼状態で実験を行った．指先に加えた力によって発生する感覚と等価な感覚量を感覚神経の電気刺激で発生させることを目的とする．この為には，指先に発生した感覚を定量評価する必要がある．今回我々は生成された感覚の計測法として，加圧した指先に発生される力と反対の指先でその力に対し等価な感覚量を提示させることとした．

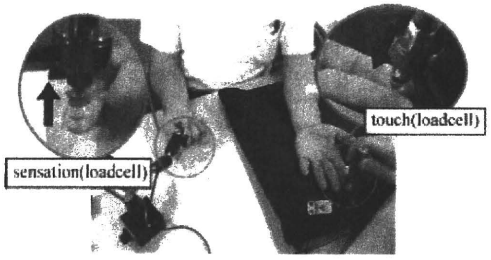

Fig.5 Quantitative evaluation of the pressure sensation evoked by microelectricqal stimulation.

3.2 機械刺激に対する感覚量

まず，片方の指先に力を加え，その力と同等の力を反対の指先で提示する実験を行った．実験結果を図 6 に示す．加圧力と感覚量の相関係数は 0.98 であり，相関が高いことから，皮膚表面に加えた機械刺激と感覚量の関係はほぼ等価な関係であることが示された．

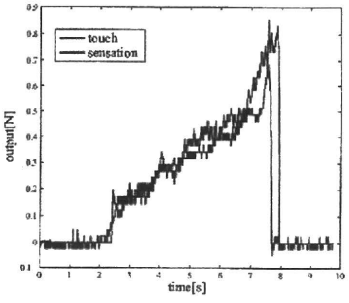

Fig.6 Actual force applied to the TPS sensor and the subjective magnitude of the evoked pressure sensation.

3.3 電気刺激に対する感覚量

次に，指先にハードカバーを装着し，感覚を遮断した状態で感覚を提示する実験を行った．FingerTPS の出力をパルス列頻度に変換・出力し，マイクロスティミュレーション法によりパルス列を神経に伝達することで感覚を提示した (図 7)．

本実験では，圧覚から電気刺激のパルス列頻度への変換式は，FingerTPS の出力 x を係数 a にて整数倍し，これをパルス頻度の周波数 f とした．即ち，$f = ax$ で，本実験では $a = 50$ とした．

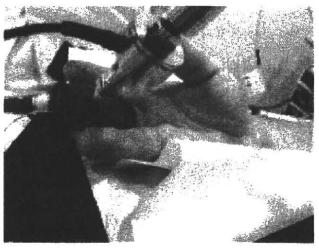

Fig.7 The manner in which a subject enhances somatic sensations by the developed system.

実験結果の一例を図 8 に示す．グラフは上から FingerTPS と加圧力と感覚量，出力周波数，出力パルスである．実験結果をみると，パルス頻度が増加することによって被験者の感覚量は増加している．押付力と感覚量の関係は相関係数 0.91 であり，高い相関があることから被験者の感覚を生成出来ていることがわかる．また，FingerTPS と押付力との相関係数は 0.97 であり，FingerTPS が接触力を忠実に再現出来ていることが確認できる．

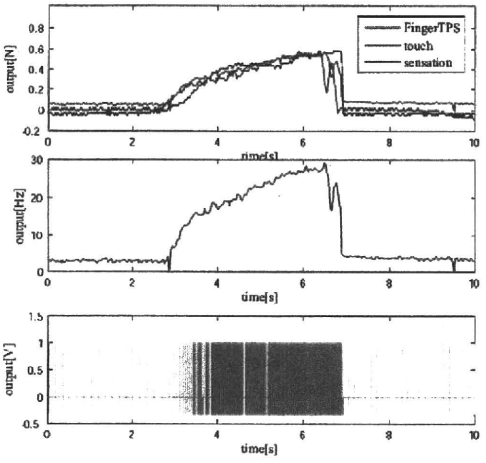

Fig.8 Response of subjective pressure sensation evoked by the microelectrical stimulation, pulse train for the microelectrical stimulation, and the actual force applied to the Finger TPS system,

4. 結言

触覚センサの出力をマイクロスティミュレーション法により神経フィードバックし，人工感覚を提示するシステムを構築した．触覚センサの出力をパルス変換し，マイクロスティミュレーション法により提示することで失われた感覚を補綴しうる可能性を示した．

文 献

[1] M.Shimojo,T.Suzuki,A.Namiki,T.Saito,M.Kunimoto, R.Makino,H.Ogawa,M.Ishikawa,K.Mabuchi "Development of a system for experiencing tactile sensation from a robot hand by electrically stimulating sensory nerve fiber" IEEE Trans.Robotics and Automation(CD-ROM),2003

[2] Kandel,Schwartz,Jessell"PRINCIPLES OF NUERAL SCIENCE Fourth Edition",McGraw-Hill,2000

[3] T.Suzuki,K.Mabuchi,H.Nishimura,T.Saito,N.Kakuta, M.Kunimoto,M.Shimojo,The Relationship between Stimulation Signals and Subjective Intensities and Areas, Proc. Int. Conf. of the IEEE EMBS,Atlanta, 459, Oct. 1999.

多層配線構造を有する神経再生型電極の開発

○吉田 充宏[1]、浮田 芳昭[1]、満渕 邦彦[2]、内海 裕一[1]
1. 兵庫県立大学高度産業科学技術研究所、2. 東京大学大学院情報理工学系研究科

1. はじめに

神経再生型電極は、末梢神経の再生現象を利用した方法であり、臨床の場ではおもに義肢等のインターフェイスとしての利用を目的とされている。原理としては、一旦切断した神経束の近位端と遠位端を、中隔を挟んで対向する形で位置させると、切断された神経軸索が近位側から再生し、電極孔を通過して末梢側に伸長して行く。これにより電極と軸策とが物理的かつ電気的に強固に固定され、電極孔を通過した再生軸索の活動測定と電気刺激が孔に設置した電極で行えるようになる。

2. 多チャンネル化可能な電極の設計

今回の設計・試作において、電極孔の大きさは神経線維の径の個体差も考慮した上で 30、60、90μm の 3 種類の大きさで、個々の電極が計測時に干渉しないように電極部の配線、配線間の幅は最小の部分で 20μm、電極部の金層の厚み 12μm と設定した。また、多チャンネル化を行うにあたり、単層での電極層では配線の密度などからチャンネル数に限界が生じる。そのため、本研究では電極層を積層させ、三次元構造とすることでの作製を試みた。積層させることで、1 層あたりでは電極を 12 個配置していたが、2 層積層することで計 24 個の電極の配置が実現可能となる(Fig.1)。

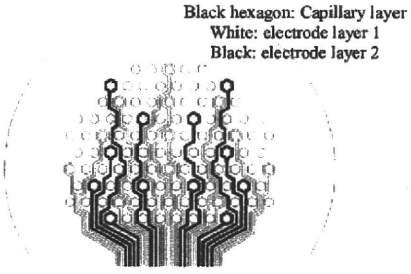

Fig.1 積層構造の電極部

3. 神経再生型電極の作製プロセス

まず、黄銅板上にレジスト AZP4903(AZ エレクトロニクスマテリアルズ(株))を用いてフォトリソグラフィにより電極部のパターニングを行い(Fig.2-a)、パターニングした部分に Au メッキをすることで電極部の作製を行い(Fig.2-b)、AZP4903 を除去することで電極部を自立させる(Fig.2-c)。そして、SU-8(日本化薬(株))のフォトリソグラフィにより絶縁層を作製し(Fig.2-d)、黄銅板を除去することで単層の電極層の作製ができる(Fig.2-e)。積層を行うため、この作業を 2 種類の電極のパターン①、②で行う。次に、積層方法については、パターン①の電極層を SiO_2 基板の上に置き(Fig.2-e)、中間の絶縁層となる SU-8 を塗布し(Fig.2-f)、パターン②の電極層とアライメントを行う(Fig.2-g)。そして、圧力をかけながら加熱を行うことで接合させる(Fig.2-h)。その後、中間層のフォトリソグラフィによりキャピラリー部を貫通させることで積層構造を有する神経再生型電極の作製ができる(Fig.2-i)。

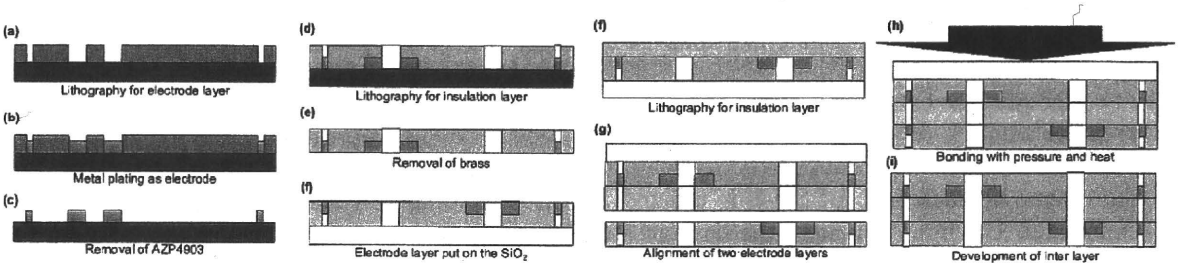

Fig.2 全工程のプロセスフロー

4. まとめ

今回作製した電極の写真を Fig.3 に示す。本研究では、神経再生型電極の多チャンネル化を実現させるため、電極層を 2 層積層することにより三次元的に作製する方法の検証を行い、それが可能であることを初めて実証した。今後は、構造パラメータの最適化と積層段の多段化、並びに作製プロセスの高度化を目指す。また、実装による実際の神経信号の計測等による検証も行っていく必要がある。

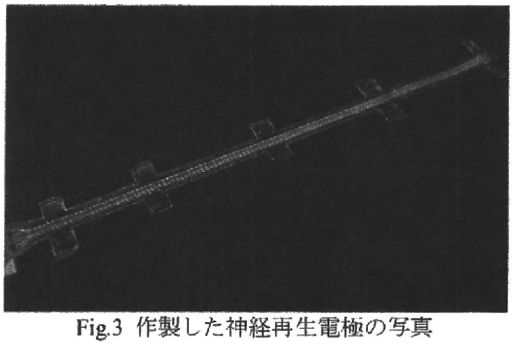

Fig.3 作製した神経再生電極の写真

Proposal of stacked electrodes for multiplex neural interface

Mitsuhiro Yoshida[1], Yoshito Hirose[1], Yoshiaki Ukita[1], Kunihiko Mabuchi[2], Yuichi Utsumi[1]
[1]Laboratory of Advanced Science and Technology for Industry, University of Hyogo,
3-1-2 Koto, Kamigori, Ako-gun, Hyogo, 678-1205, Japan
[2]Graduate School of Information Science and Technology, The University of Tokyo,
7-1-3, Hongo, Bunkyo-ku, Tokyo, 113-8656, Japan
Phone: +81-791-58-0232, Fax: +81-791-58-0232, E-mail: mituhiro@lasti.u-hyogo.ac.jp

Information on the nervous system is expressed by the trains of action potentials transmitted through the axons from neurons and this neural signal can be detected by mounting electrodes close to the nerve fibers or nerve cells. Also, nerve signals can be generated by stimulating the nerve cells or nerve fibers [1]. Recently such technology has become widely used not only for brain machine interface (BMI) systems in clinical medicine but also for investigating nervous functions in the field of basic neural sciences. In such fields, in addition to analyzing nerve signals of a single neuron or single axon, it is also very important to analyze neural information expressed by network-level in the nervous system. Key to doing this is developing neural electrodes that can record and/or stimulate neurons or axons simultaneously with many channels. Thus, a nerve regeneration electrode system is proposed as a candidate for such electrodes [2]. This electrode is designed for recording signals of peripheral nervous system and uses peripheral nerve regeneration. The concept of the electrode is as follows (see Fig.1). We cut a peripheral nerve trunk once and face the proximal stump and distal stump towards each other in a guide tube for regeneration. At this time, between the two stumps we put a septum with many holes that all electrode sites. Then cut axons begin to regenerate and extend from the proximal side, pass through the electrode holes of the septum, and it has thus become possible to measure the electrical activity of the axons or simulate them electrically by using the electrode holes.

A very serious problems with the nerve regeneration electrode is wiring from/to the electrode sites. The nerve regeneration electrode must be equipped with a huge number of electrode channels, which means that the wiring to and from the electrode holes has inevitably become very complex. In this study, we designed and manufactured a regeneration electrode with which we can solve the upper-mentioned wiring problem by using the stacked structure of the electrodes. Figure 2 (a) outlines the schematic diagram of the nerve regeneration electrode. To increase the number of electrodes we propose a stacked electrode structure. It is difficult to integrate many electrodes by using single layer due to the restriction of the integration of each electrode area. Thus the electrode shape is designed to be stacked, enabling three-dimensional (3D) inter connection of multiple electrode lines. The first attempt achieved two designed electrode structures with 12 channels stacked on a substrate and total 24 channels. Figure 2 (b) shows the designed nerve reproduction electrodes.

The proposed stacked electrodes were fabricated on the basis of multiple stacking SU-8-layers [3]. The prepared single layer electrode chips were piled up together by using precise alignment and bonding processes. Figure 3 shows the fabrication process image of bonding. To bond the electrodes without bounding reagent, the unique characteristic of SU-8 is utilized for the patterning of capillaries and bonding. The SU-8 was exposed to UV light to pattern the through hole structure, achieving stronger bonding between two bonded surfaces. Figure 4 (a) shows the outer view of fabricated electrodes. Figure 4 (b) zooms in on the structure of electrodes. As shown in Fig.4 (b), the three-dimensionally stacked electrodes and through capillary for nerve growth are successfully aligned and patterned in monolithic SU-8 chip. We developed the method to manufacture a three-dimensional electrodes structure to realize the multi channel for the flexible-regeneration nerve electrode. The structure parameter and the stacking step of the fabrication process need to be further optimized evaluated by adapting it to the measurement of an actual neural coding with mounting on animals.

REFERENCES

[1] Å. B. Vallbo, K. E. Hagbarth, and B. G. Wallin, J Apply Physiol, Vol. 96, pp.1262-1269 (2004)
[2] T. Suzuki, T. Saito and K. Mabuchi, Technical report of IEICE, Vol. 100, No. 479 pp.63-66 (2000)
[3] F. J. Blanco, M. Agirregabiria, J. Garcia, J. Berganzo, M. Tijero, M. T. Arroyo, I. Aramburu and K. Mayora, J.Micromech. Microeng, Vol. 14, pp.1047-1056 (2004)

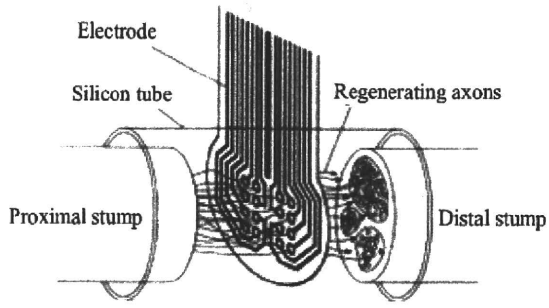

Fig.1 Model of nerve regeneration electrode

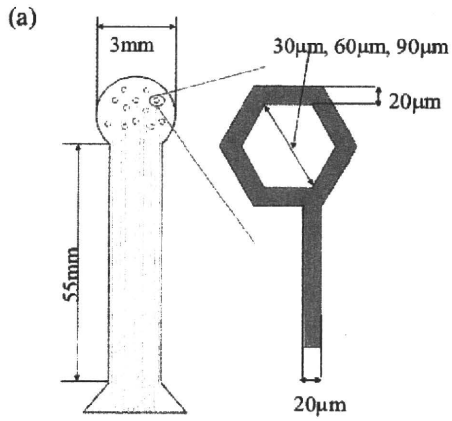

Black hexagon: capillary layer
White: electrode layer 1
Black: electrode layer 2

Fig.2 (a) Outline of electrode
(b) Designed nerve regeneration electrodes

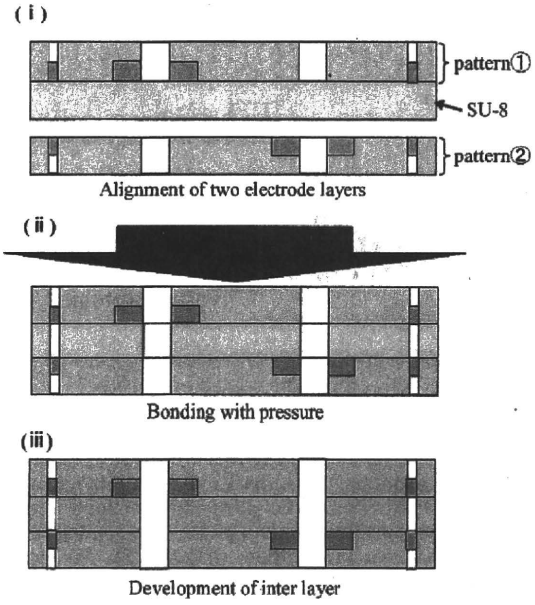

Fig.3 Fabrication process image of bonding

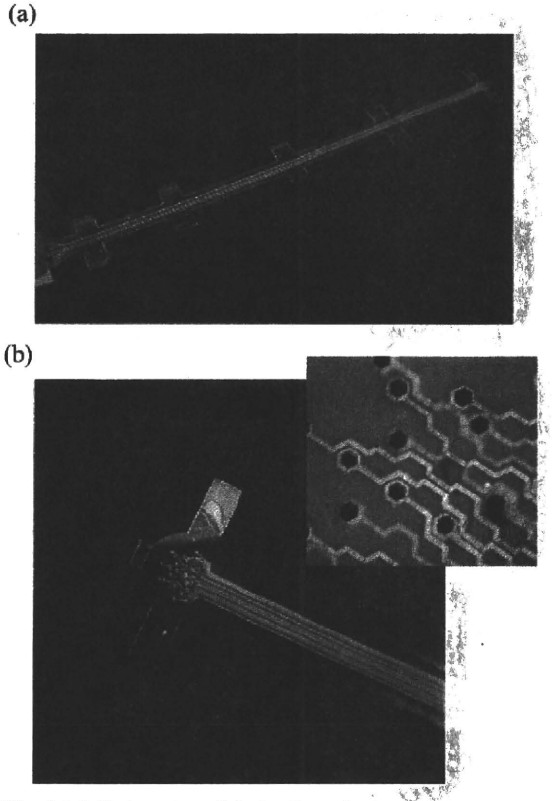

Fig.4 (a) Outer view fabrication electrodes
(b) Zoom in on structure of electrodes

Phase-Compensated Averaging for Analyzing Electroencephalography and Magnetoencephalography Epochs

Ayumu Matani*, *Member, IEEE*, Yasushi Naruse, Yasushi Terazono, Taro Iwasaki, Norio Fujimaki, *Member, IEEE*, and Tsutomu Murata

***Abstract*—Stimulus-locked averaging for electroencephalography and/or megnetoencephalography (EEG/MEG) epochs cancels out ongoing spontaneous activities by treating them as noise. However, such spontaneous activities are the object of interest for EEG/MEG researchers who study phase-related phenomena, e.g., long-distance synchronization, phase-reset, and event-related synchronization/desynchronization (ERD/ERS). We propose a complex-weighted averaging method, called phase-compensated averaging, to investigate phase-related phenomena. In this method, any EEG/MEG channel is used as a trigger for averaging by setting the instantaneous phases at the trigger timings to 0 so that cross-channel averages are obtained. First, we evaluated the fundamental characteristics of this method by performing simulations. The results showed that this method could selectively average ongoing spontaneous activity phase-locked in each channel; that is, it evaluates the directional phase-synchronizing relationship between channels. We then analyzed flash evoked potentials. This method clarified the directional phase-synchronizing relationship from the frontal to occipital channels and recovered another piece of information, perhaps regarding the sequence of experiments, which is lost when using only conventional averaging. This method can also be used to reconstruct EEG/MEG time series to visualize long-distance synchronization and phase-reset directly, and on the basis of the potentials, ERS/ERD can be explained as a side effect of phase-reset.**

***Index Terms*—Alpha rhythm, alpha ringing, averaging, electroencephalography (EEG), event-related synchronization/desynchronization (ERS/ERD), long-distance synchronization, megnetoencephalography (MEG), phase-reset.**

Manuscript received July 17, 2009; revised October 9, 2009 and November 27, 2009. First published February 17, 2010; current version published April 21, 2010. This work was supported in part by a grant-in-aid for scientific research (B) from the Ministry of Education, Science, Sports and Culture under Grant 21300102. *Asterisk indicates corresponding author.*

*A. Matani is with the Graduate School of Frontier Sciences, the University of Tokyo, Kashiwa 277-8561, Japan, and also with the Biological ICT Group, National Institute of Information and Communication Laboratory, Kobe 651-2492, Japan (e-mail: matani@isp.ac).

Y. Naruse and T. Murata are with the Biological ICT Group, National Institute of Information and Communication Laboratory, Kobe 651-2492, Japan.

Y. Terazono and T. Iwasaki are with Graduate School of Frontier Sciences, the University of Tokyo, Kashiwa 277-8561, Japan.

N. Fujimaki is with the Biological ICT Group, National Institute of Information and Communication Laboratory, Kobe 651-2492, Japan, with Graduate School of Life Science and Systems Engineering, Kyushu Institute of Technology, Kitakyushu 808-0196, Japan, and also with the Human Information System Laboratories, Kanazawa Institute of Technology, Kanazawa, Ishikawa 921-8501, Japan.

Color versions of one or more of the figures in this paper are available online at http://ieeexplore.ieee.org.

Digital Object Identifier 10.1109/TBME.2009.2038363

I. Introduction

STIMULUS-LOCKED averaging (conventional averaging, hereafter) is often used for analyzing electroencephalography (EEG) and magnetoencephalography (MEG) epochs to enhance the signal-to-noise ratio (SNR). However, EEG and MEG (xEG, hereafter) researchers differ in their concepts of signal and noise. Spontaneous activities, which are observed as rhythmic activities in each epoch, are canceled out by conventional averaging, since they are not stimulus-locked. The mean xEG time series, or the stimulus-evoked activity in the narrow sense, is considered to be the signal, and ongoing spontaneous activities are considered to be noise.

On the contrary, xEG researchers who study phase-related phenomena, e.g., long-distance synchronization, phase-reset, and event-related synchronization/desynchronization (ERS/ERD), are rather interested in ongoing spontaneous activities. Some xEG researchers think that the mean time series is not stimulus-evoked but stimulus-induced via a phase-reset of ongoing spontaneous activity [1], and there is a relationship between phase-reset and alpha ringing, which is the alpha-band synchronization appearing around 0.5–0.9 s after stimulus onset [2]. Some xEG researchers believe that ERS/ERD of ongoing spontaneous activity plays a functional role [3]. Some xEG researchers are interested in the rhythmic synchronization between distant brain areas, called long-distance synchronization [4]. The amount of synchronization has been evaluated by using an index called the phase-locking value (PLV). Recently, the directional relationship between two brain areas has been investigated via phase synchronization [5]. The directional relationship has been quantitatively evaluated by using an index, called the Granger causality spectra, based on a multivariate autoregressive model. The ongoing spontaneous activities are considered to be signals, and therefore, conventional averaging is not appropriate for their analyses.

Can the ongoing spontaneous activities be averaged instead of averaging the stimulus-evoked activity? Also, can the directional relationship of ongoing spontaneous activities between xEG channels be evaluated as an xEG time series not instead of as an index? If such an xEG time series can be obtained, conventional analyses for processing xEG time series (e.g., solving xEG inverse problem) can be applied to it.

In this paper, we propose an extended stimulus-locked averaging method, called phase-compensated averaging. This method

seeks to average an ongoing spontaneous rhythm and to evaluate the directional phase-synchronizing relationship between xEG channels by setting any xEG channel as a trigger channel.

II. Method

A. Concept of Phase-Compensated Averaging

External triggering for conventional averaging is usually performed by using a time series generated by an external device for stimulation. The trigger timings are determined by the characteristics of the time series. The timings at which the amplitude exceeds a specific threshold value will be the trigger timings. Therefore, a pulse train, which has no essential meaning for stimulation, is often employed as the time series for triggering.

On the other hand, internal triggering is often used for averaging electrocardiography (ECG) and/or magnetocardiography (MCG) epochs. The trigger timings are determined by the characteristics of a single ECG/MCG (xCG, hereafter) epoch. For instance, the timings at which the amplitude of QRS complexes reach individual peaks can be used as the trigger timings.

In external and internal triggering, trigger timings are determined by the amplitude characteristics of the time series. Assuming that the time series is complex-valued, phase characteristics can alternatively be used. For instance, the timings at which the phase of the time series reaches a specific value can be used as the trigger timings.

Unfortunately, a single xEG epoch does not have conspicuous amplitude characteristics like those of single xCG epoch. Therefore, to find reliable trigger timings, internal triggering based on amplitude is not appropriate, and we may be forced to use external triggering based on amplitude. However, internal triggering based on phase can be associated with external triggering based on amplitude; i.e., xEG epochs can be compensated such that their instantaneous phases at the external trigger timings are set to a specific value. This phase compensation is worth considering at least for the following reason. Conventional averaging cancels out ongoing spontaneous activities on the basis of the fact that the instantaneous phases of epochs at the external trigger timings are uniformly distributed. If these phases are compensated to lock in a specific value, ongoing spontaneous activities should appear with a high SNR after averaging.

B. Procedure of Phase-Compensated Averaging

Fig. 1 shows a schematic diagram of phase-compensated averaging. Preprocessing [see Fig. 1(a)] is done prior to averaging [see Fig. 1(b)].

In Fig. 1(a), the xEG time series of the lth channel, qth epoch ($q = 0,1,\ldots,Q-1$), and nth time sampling point is denoted by $x_{lq}[n]$ ($n = 0$ is the external trigger timing). First, $x_{lq}[n]$ is narrow-band filtered to get $x^{\mathrm{N}}_{lq}[n]$. The passband is selectable. For instance, if xEG researchers are interested in the alpha-band phase modulation, the frequency from the alpha to beta band, taking the frequency shift by the phase modulation into account, would be the best choice. Second, $x^{\mathrm{N}}_{lq}[n]$ is discrete Hilbert transformed [7] to get $\tilde{x}^{\mathrm{N}}_{lq}[n]$, which is a complex-valued xEG of $x^{\mathrm{N}}_{lq}[n]$, and the instantaneous phase is simply determined as

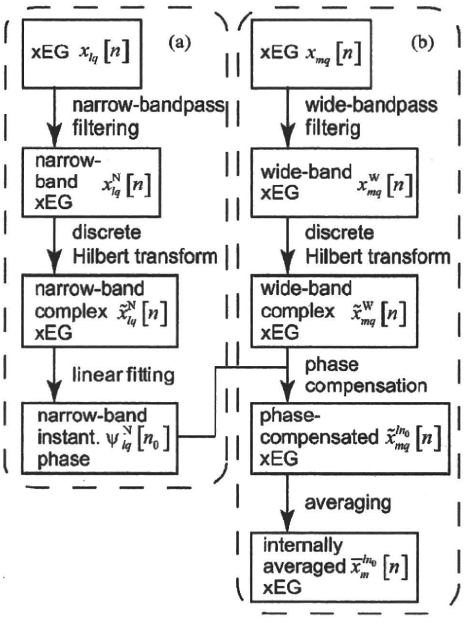

Fig. 1. Schematic diagram of phase-compensated averaging. (a) Instantaneous phase of the narrow-band xEG of the lth channel and the qth epoch at the n_0th time sampling point $\psi^{\mathrm{N}}_{lq}[n_0]$ is calculated. (b) Average of the wide-band xEG of the mth channel compensated by $\psi^{\mathrm{N}}_{lq}[n_0]$, $\bar{x}^{ln_0}_{m}[n]$, is calculated.

$\mathrm{Arg}\{\tilde{x}^{\mathrm{N}}_{lq}[n]\}$. Since the discrete Hilbert transform (DHT) is actually zero-padding in the frequency domain, narrow-bandpass filtering can be involved in DHT by padding additional zeros to the stopband. Finally, the instantaneous phase at time sampling point n_0, $\psi^{\mathrm{N}}_{lq}[n_0]$, is precisely calculated by using a least squares fit of the first-order polynomial to the instantaneous phase in duration G, $\mathrm{Arg}\{\tilde{x}^{\mathrm{N}}_{lq}[n]\}_{n\in G}$, where n_0 is the center time sampling point in G and will be the trigger timing. G is set to one period of the frequency band of interest to fit the narrow-band, e.g., 0.1 s for fitting to the alpha band. Note that the only production in the series of procedures in Fig. 1(a) is $\psi^{\mathrm{N}}_{lq}[n_0]$, and hence $\tilde{x}^{\mathrm{N}}_{lq}[n]$ is no longer used.

In Fig. 1(b), the procedure for obtaining a wide-band complex-valued xEG $\tilde{x}^{\mathrm{W}}_{mq}[n]$ of the mth channel is the same as in Fig. 1(a), except for the passband. This passband is set to the one that xEG researchers usually select, and hence, it is relatively wide-band. $\tilde{x}^{\mathrm{W}}_{mq}[n]$ is phase-compensated by $\psi^{\mathrm{N}}_{lq}[n_0]$ as

$$\tilde{x}^{ln_0}_{mq}[n] = \tilde{x}^{\mathrm{W}}_{mq}[n]\exp\left(-\mathrm{j}\psi^{\mathrm{N}}_{lq}[n_0]\right) \tag{1}$$

where j is the imaginary unit. The phase compensation (1) indicates that the mth channel xEG is compensated such that the instantaneous narrow-band phase of the lth channel is 0 at n_0. Since $\tilde{x}^{\mathrm{W}}_{mq}[n]$ is complex-valued, this compensation is actually a rotation on the complex plane. Finally, we obtain the average of the mth channel compensated by the lth channel as

$$\bar{x}^{ln_0}_{m}[n] = \frac{1}{Q}\sum_{q=0}^{Q-1}\tilde{x}^{ln_0}_{mq}[n]. \tag{2}$$

The DHT for determining the narrow-band instantaneous phase $\psi_{lq}^{\mathrm{N}}[n_0]$ [see Fig. 1(a)] can be replaced with a wavelet-based method [2], [4]. The difference between the results of these two methods is minor [9]. However, a sort of integration of the phases in the narrow-band is necessary for a wavelet-based method to determine a representative phase. The reason for employing DHT is that it involves such an integration. The aforementioned procedure of phase-compensated averaging was implemented in MATLAB.

C. Auto and Cross Averages

Phase-compensated averaging embodies a new concept, auto and cross averages. We call the case of $l = m$ in averaging (2) auto average and the case of $l \neq m$ cross average. In phase-compensated averaging, any xEG channel can be used for internal triggering, so there is no need to distinguish internal and external channels. Accordingly, the conventional average is a cross average compensated by the external trigger channel.

We would like to emphasize that cross averaging is directional, namely $\bar{x}_m^{ln_0}[n] \neq \bar{x}_l^{mn_0}[n]$. Therefore, phase-compensated averaging can selectively average ongoing spontaneous activity phase-locked in any xEG channel. In other words, phase-compensated averaging can evaluate the directional relationship of ongoing spontaneous activities between xEG channels as xEG time series.

D. Another Interpretation

The phase-compensated average is approximated by the first term of the discrete Fourier transform of over sorted epochs as follows. Since stimuli are repeatedly presented with random timings, instantaneous phases are uniformly distributed from 0 to 2π in the case that n_0 is chosen at a pretrigger time sampling point. Now, let $\eta[q]$ be the epoch order permutation function that sorts the epochs in ascending order of $\psi_{lq}^{\mathrm{N}}[n_0]$ from 0 to 2π. We have the following approximation:

$$\psi_{l\eta[q]}^{\mathrm{N}}[n_0] \simeq \frac{2\pi q}{Q}. \tag{3}$$

Substituting approximation (3) into the phase-compensated average (1) and (2), we obtain an interpretation of this averaging with the first term of the discrete Fourier transform

$$\bar{x}_m^{ln_0}[n] \simeq \frac{1}{Q}\sum_{q=0}^{Q-1} \tilde{x}_{m\eta[q]}^{\mathrm{W}}[n] \exp\left(-\mathrm{j}\frac{2\pi lq}{Q}\right). \tag{4}$$

Fourier form (4) immediately leads to the interpretation that the conventional average corresponds to the zeroth term of the discrete Fourier transform. Phase-compensated averaging is an extension of conventional averaging.

This Fourier interpretation introduces the concept of signal and noise. The power of epochs in the time domain is distributed over the epochs in the frequency domain in the sense of Parseval's theorem. While using only conventional averaging treats the first and higher terms as noise, simultaneous use of conventional and phase-compensated averaging treats the second and higher terms as noise. This means information that would otherwise be lost by performing only conventional averaging can be recovered by using phase-compensated averaging.

III. Simulation I: Fundamental Characteristics

A simulation was performed to reveal the fundamental characteristics of phase-compensated averaging.

A. Given Epochs

Two-channel ($m = 1, 2$) and 200-trial ($q = 0, 1, \ldots, 199$) xEG epochs $x_{mq}(t)$, $(-0.2 \leq t \leq 0.5\,\mathrm{s})$, were given as

$$x_{mq}(t) = x^{\mathrm{EV}}(t) + x_{mq}^{\alpha}(t) + R_{mqt}^{\mathrm{N}}(0, 0.3) \tag{5}$$

where

$$x^{\mathrm{EV}}(t) = \exp(-5 \times 10^3 (t - 0.1)^2) + 0.5\exp(-10^3(t - 0.2)^2) \tag{6}$$

is the common stimulus-evoked activity, $x_{mq}^{\alpha}(t)$ is alpha-band activity having trial-wise different initial phases, and $R^{\mathrm{N}}(a, b)$ is additive noise in the form of normally distributed random numbers with mean a and standard deviation b with respect to each of the subscripts (m, q, and t).

Let us explain $x_{mq}^{\alpha}(t)$ in detail. $x_{mq}^{\alpha}(t)$ includes directional phase modulation from channel 1 to channel 2 as follows. First, the phases of $x_{mq}^{\alpha}(t)$ are prepared as

$$\theta_{1q}(t) = \psi_{1q}(t)$$

$$\theta_{2q}(t) = \begin{cases} \psi_{2q}(t), & t \leq 0.1 \\ (\psi_{1q}(0.3) - \psi_{2q}(0.1))(t - 0.1)/0.2 + \psi_{2q}(0.1), & 0.1 < t \leq 0.3 \\ \psi_{1q}(t), & 0.3 < t \end{cases} \tag{7}$$

where

$$\psi_{mq}(t) = 2\pi 10t + R_{mq}^{\mathrm{U}}(0, 2\pi) \tag{8}$$

and $R_{mq}^{\mathrm{U}}(0, 2\pi)$ denotes uniformly distributed random numbers from 0 to 2π with respect to m and q. $R_{mq}^{\mathrm{U}}(0, 2\pi)$ is the initial phase difference. The phases of channel 2 are connected to those of channel 1 with straight lines for the duration from 0.1 to 0.3 s, as shown in the top row of Fig. 2. These phase connections are random because of $R_{mq}^{\mathrm{U}}(0, 2\pi)$. Thus, the phases of channel 2 are unilaterally drawn into those of channel 1. Finally, the alpha-band activities are constructed as

$$x_{mq}^{\alpha}(t) = R_{mq}^{\mathrm{N}}(1, 0.3)\cos\left(\theta_{mq}(t) + R_{mqt}^{\mathrm{N}}(0, 0.3\pi)\right) \tag{9}$$

where $R_{mq}^{\mathrm{N}}(1, 0.3)$ and $R_{mqt}^{\mathrm{N}}(0, 0.3\pi)$ are amplitude-modulation and additive phase noise. The bottom row of Fig. 2 shows typical examples of given epochs of channels 1 and 2. These epochs are very noisy, so the stimulus-evoked activity cannot be observed directly.

The simulation was performed with a sampling frequency of 1 kHz.

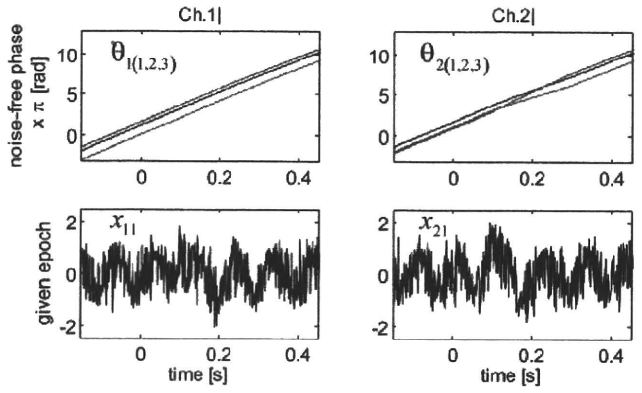

Fig. 2. Settings of Simulation I. (left column) xEG time series of channel 1. (right column) xEG time series of channel 2. (top row) Stacked given phases without noise for the first three epochs. (bottom row) Given xEG time series for the first epoch.

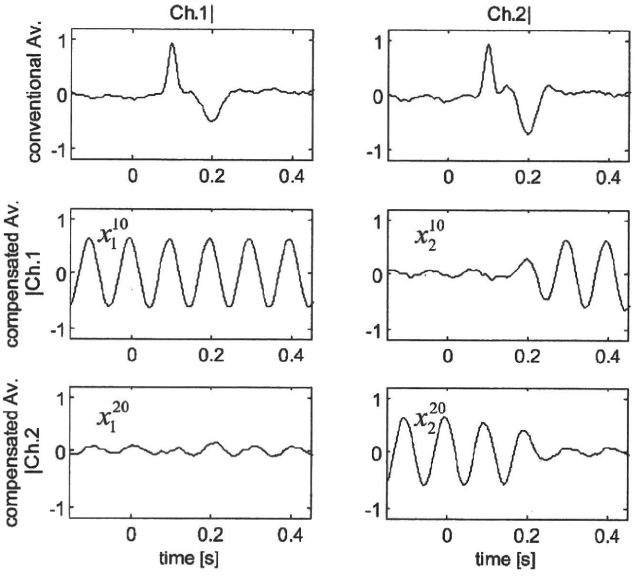

Fig. 3. Results of Simulation I. (left column) xEG time series of channel 1. (right column) xEG time series of channel 2. (top row) Conventional averages. (middle row) averages compensated by instantaneous phases of channel 1. (bottom row) Averages compensated by instantaneous phases of channel 2.

B. Conventional Averages

The top row of Fig. 3 shows the conventional averages of channels 1 and 2. The given ongoing alpha-band activities are almost canceled out in both channels. The stimulus-evoked activities of channels 1 and 2 were extracted without and with distortion, respectively. The difference between channels is due to the directional phase modulation from channel 1 to channel 2. In the meantime of the phase modulation, the instantaneous phases of the given epochs were not uniformly distributed from 0 to 2π. Therefore, the conventional average included stimulus-induced activities via the phase modulation.

C. Phase-Compensated Averages

Phase-compensated averaging was performed under the following conditions. The passband for narrow-bandpass filtering and the duration G [both in Fig. 1(a)] were 8–26 Hz (from alpha- to beta-band) and -0.05 to 0.05 s. The instantaneous phases were calculated at $n_0 = 0$ s. The passband for wide-bandpass filtering was 1–52 Hz [see Fig. 1(b)]. Both narrow- and wide-bandpass filtering were performed as part of the DHT by padding additional zeros to the stopbands.

The bottom two rows show the phase-compensated averages in 2×2 matrix form; i.e., the columns indicate channels for averaging [m in phase-compensated average (2)], and the rows indicate channels for the instantaneous phase calculation [l in phase-compensated average (2)]. Thus, the "diagonal" and "off-diagonal" panels indicate auto and cross averages, respectively. Note that only the real parts are presented because phase-compensation (1) rotates the narrow-band part of the complex xEG epochs onto the real axis. Although the auto average $\bar{x}_1^{10}[n]$ showed stable alpha-band activity all the time, the auto average $\bar{x}_2^{20}[n]$ decayed after 0.2 s. On the other hand, although the cross average $\bar{x}_1^{20}[n]$ showed small activity all the time, the cross average $\bar{x}_2^{10}[n]$ increased in amplitude after 0.1 s. The reason these phenomena occurred was that channel 2 was modulated by channel 1 for 0.1–0.2 s but channel 1 was not influenced by channel 2 all the time under phase setting (7). Therefore, phase-compensated averaging revealed not only the relationship between channels 1 and 2 but also their directional relationship, namely from channel 1 to channel 2.

To avoid having the stimulus-evoked activity leak into the phase-compensated averages, the duration G should be one in which the instantaneous phases over epochs are almost uniformly distributed. In such a selection, the average of the stimulus-evoked activity complex-weighted with uniformly distributed phases will theoretically be zero, since the stimulus-evoked activity is common to all epochs. Accordingly, the ongoing spontaneous activities can be selectively averaged in the phase-locking sense by using the parameters of the instantaneous phase calculation.

IV. Simulation II: Stimulus-Induced Activities via Changes of Ongoing Spontaneous Activities

Two simulations were performed to analyze stimulus-induced activities via changes of ongoing spontaneous activities. The additive stimulus-evoked activity and random numbers used in Simulation I were not given. Since the given xEG epochs of both simulations in Simulation II were noise-free and narrow-band, narrow- and wide-bandpass filtering were not performed. The sampling frequency was 1 kHz and the duration G for determining the instantaneous phases was -0.35 to -0.25 s (namely, $n_0 = -0.3$ s).

A. Phase-Reset

Unlike the random phase modulation in Simulation I, a systematic phase modulation to simulate a phase-reset was prepared. First, single-channel and 200-trial ($q = 0, 1, \ldots, 199$)

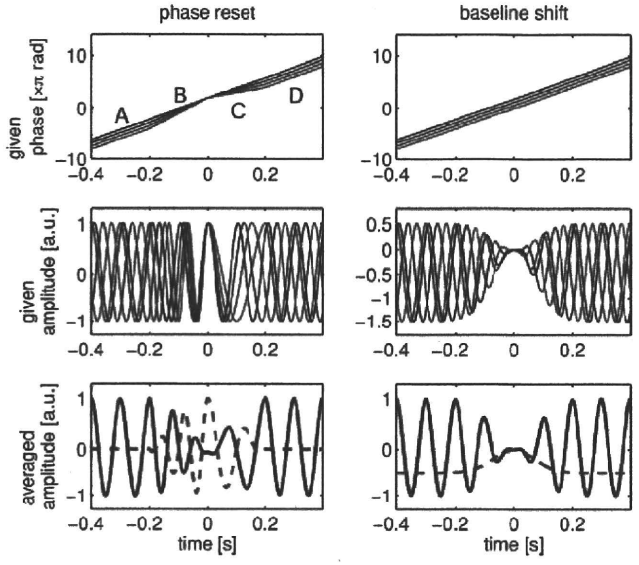

Fig. 4. Simulation II for xEG generation models. (left column) Phase reset model. (right column) Baseline shift model. (top row) Stacked given phases (q = 0, 60, 120, 180). (middle row) Stacked given xEG time series (q = 0, 60, 120, 180). (bottom row) Results of Simulation II. The dashed and solid lines indicate conventional averaging and phase-compensated averaging results, respectively.

phases are given as

$$\theta_q^{\mathrm{PR}}(t) = \begin{cases} \psi_q^{\mathrm{PR}}(t), & t \le -0.2,\ 0.2 < t \\ (\psi_{199}^{\mathrm{PR}}(0) - \psi_q^{\mathrm{PR}}(-0.2))t/0.2 + \psi_{199}^{\mathrm{PR}}(0), & -0.2 < t \le 0 \\ (\psi_{199}^{\mathrm{PR}}(0.2) - \psi_q^{\mathrm{PR}}(0))t/0.2 + \psi_{199}^{\mathrm{PR}}(0), & 0 < t \le 0.2 \end{cases} \tag{10}$$

where

$$\psi_q^{\mathrm{PR}}(t) = 2\pi 10t + \frac{2\pi q}{200}. \tag{11}$$

Here PR stands for phase reset. The top-left panel in Fig. 4 illustrates four samples of the given phase (10). The phases that were uniformly distributed in duration A (−0.4 to −0.2 s) linearly changed to a point distribution in duration B (−0.2 to 0 s), and *vice versa* in durations C (0–0.2 s) and D (0.2–0.4 s). The xEG epochs are given as

$$x_q^{\mathrm{PR}}(t) = \cos\theta_q^{\mathrm{PR}}(t). \tag{12}$$

The middle-left panel in Fig. 4 illustrates the four samples of the given epochs. The phases were locked at 0 s.

The bottom-left panel shows the conventional and phase-compensated average. While the conventional average revealed the stimulus-induced activity via the phase-reset, the phase-compensated average revealed the phase modulation of the phase-reset; the amplitudes of these averages changed complementarily, and therefore, the conventional average was not caused by stimulus-evoked, or additive, activities. These averages also revealed upward (duration B) and downward (duration C) shifts in frequency. These shifts were coincident with the given phases. Note that the time derivative of phase is frequency.

B. Baseline Shift

A third xEG generation model has been recently proposed [8]. In this model, the conventional average, or the mean time series, is stimulus-induced via an amplitude modulation of a baseline-shifted ongoing spontaneous activity.

The single-channel and 200-trial (q = 0, 1, ..., 199) xEG epochs follow

$$x_q^{\mathrm{BS}}(t) = (1 - \exp(-100t^2))\left(\cos\psi_q^{\mathrm{PR}}(t) - 0.5\right) \tag{13}$$

associated with equally spaced phases (11). BS stands for baseline shift. The top- and middle-right panels in Fig. 4 illustrate the given phases and epochs, respectively. The figures show an amplitude modulation rather than a phase modulation. The bottom-right panel shows the conventional and phase-compensated averages. Similar to the phase-reset simulation, the amplitudes of these averages changed complementarily, and therefore, the conventional average was not caused by the stimulus-evoked activities. However, unlike the phase-reset simulation, these averages successfully revealed the amplitude modulation but no phase modulation.

V. Results and Discussion

We applied this method to an offline analysis of a simple EEG experiment to determine whether information lost by using only conventional averaging can be recovered or not.

A. EEG Recording

Three subjects experienced three runs of flash stimuli, each of which consisted of 200 flashes (stimulus onset timing: 0 s, flash duration: 0.033 s, stimulus onset asynchrony: 2–3 s random). They received instructions just before each run; i.e., they were asked in Run 1) to view the flashes passively, in Run 2) to press a button as soon as they recognized the flashes, and in Run 3) to view them passively again. Thus, Runs 1–3 had no essential differences as stimuli and that Runs 1 and 3 were the same even with their instructions.

During these runs, 31-channel EEG (extended international 10–20 system) was simultaneously recorded with a sampling frequency of 1.2 kHz. Phase-compensated averaging used the same passbands, duration G, and timing n_0, as in Simulation I.

The subjects gave written informed consent after a detailed explanation of this study. The study received ethical approval from the Ethics Committee for Human and Animal Research of the Graduate School of Frontier Sciences, the University of Tokyo.

The scope of this paper is not to discuss brain functions but to describe a new averaging method. Hence, it is enough for our purpose to present an analysis of two-channel EEG (FCz: located at frontal point on the medial line, Oz: located at the occipital point on the medial line) for a typical subject.

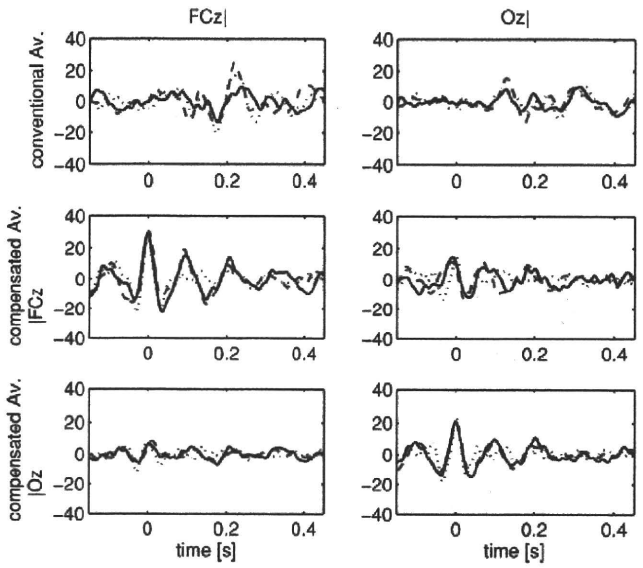

Fig. 5. Phase-compensated averages of a flash evoked potential. In all six panels, the dotted, dashed, and solid lines indicate EEG time series from Runs 1, 2, and 3, respectively. (left column) EEG time series of FCz (a frontal channel). (right column) EEG time series of Oz (an occipital channel). (top row) Conventional averages. (middle row) Averages compensated by instantaneous phases of FCz. (bottom row) Averages compensated by instantaneous phases of Oz.

B. Conventional Averages

The top-row of Fig. 5 shows conventional averages of FCz and Oz. For both channels, Run 2 showed a large activity and Run 3 showed a small activity relative to Run 1. The conventional averages of both channels for Run 3 were rather similar to those for Run 1 in terms of the waveform. This implies that button pressing and attention to this task increased activity in Run 2 and habituation decreased activity in Run 3. However, these speculations are not important; only amplitude and similarity relations among Runs 1–3 are relevant to our purpose.

C. Phase-Compensated Averages

The middle and bottom rows of Fig. 5 show compensated averages of FCz and Oz. The presentation style is the same as in Fig. 3.

The auto averages of both channels for Run 3 showed large activities. Moreover, the EEG time series of the auto averages for Run 3 were similar to those for Run 2 in terms of the waveform.

On the other hand, the cross averages of Oz compensated by FCz showed larger activities than those of FCz compensated by Oz. This implied that the directional relationship, or an information flow, from frontal (FCz) to occipital (Oz) was more prominent than from Oz to FCz. Although the reverse direction is believed to be a visual pathway, information flow from frontal to occipital has been also reported [6]. Putting the issue of the direction aside, we note that cross averages are useful for revealing such a directional relationship. Moreover, the auto averages of both channels for Run 3 were also similar to those for Run 2 in terms of the waveform.

Regarding the auto and cross averages, Run 3 had amplitude and similarity relations different from those obtained by only conventional averaging. This implies that information regarding Run 3 that cannot be explained by only habituation and may be affected by the experience of Run 2, was revealed by phase-compensated averaging. Note that the important point here is not speculation about brain functions but potential of this method to recover information.

D. Relationship Between Phase-Compensated Averages and Phase-Related Phenomena

As shown in the phase-compensated averages of channels 1 and 2 (see Fig. 3) and those of FCz and Oz (see Fig. 5), long-distance directional synchronizations were investigated by looking at the cross averages. Although we applied this method directly to EEG epochs to avoid a discussion nonessential to propose this method, this method can be applied to epochs that closely reflect brain activities (e.g., electrocorticogram (ECoG) and inverse solutions of xEG) without any modification.

If long-distance directional phase synchronization between two brain areas occurs, one must phase-synchronize to the other. In the meantime, a phase-reset must also occur. Note that phase-reset here does not mean the well-known phase-reset in which instantaneous phases jump to a specific value like in Simulation II, but rather a sort of drawing phenomenon that occurs between channels 1 and 2 in Simulation I. Phase-compensated averaging can detect both types of phase-reset.

Let us briefly discuss ERS/ERD because phase-compensated averaging does not directly visualize ERS/ERD. If the phase-reset similar to Simulation I occurs mainly in the alpha rhythms, the beta- and gamma-rhythms are generated in the transient phase-locking duration. These phenomena may be observed as ERS/ERD. In fact, a phase with a slope steeper than the alpha band appears in the top-right panel of Fig. 2.

The alpha-band activity often observed in phase-compensated averages, which in fact appears in Fig. 5, should be treated as a kind of alpha ringing. This is because alpha ringing is observed in conventional averages, which are interpreted as cross averages that are phase-compensated by the external trigger channel.

VI. Conclusion

We presented a complex-weighted averaging method, called phase-compensated averaging, to reveal amplitude and phase modulations of the target ongoing spontaneous activity, e.g., alpha rhythm. In this method, the instantaneous phases of xEG epochs at a specific time are first calculated. The specific time must be chosen such that the instantaneous phases are uniformly distributed from 0 to 2π. By making a suitable choice, the phase-compensated averages can reveal the modulations without the leakage of the purely stimulus-evoked activity while the conventional averages suffer from the leakage of the phase modulation. However, since the relationship between conventional averaging and phase-compensated averaging is complementary as shown in Simulations I and II, simultaneous use of these averages would be useful for analyzing the stimulus-evoked and/or stimulus-induced xEG activities. Note that we do not

infer the existence of the stimulus-evoked, or additive, activity. Moreover, phase-compensated averaging can reveal the directional phase synchronization between a pair of xEG channels. This characteristic would be useful for analyzing the directional relationship among xEG channels.

REFERENCES

[1] S. Makeig, M. Westerfield, T. P. Jung, S. Enghoff, J. Townsend, E. Courchesne, and T. J. Sejnowski, "Dynamic brain sources of visual evoked responses," *Science*, vol. 295, pp. 690–694, 2002.

[2] Y. Naruse, A. Matani, T. Hayakawa, and N. Fujimaki, "Influence of seamlessness between pre- and post stimulus alpha rhythms on visual evoked potential," *NeuroImage*, vol. 32, pp. 1221–1225, 2006.

[3] C. Tallon-Baudry and O. Bertrand, "Oscillatory gamma activity in humans and its role in object representation," *Trends Cognitive Sci.*, vol. 3, pp. 151–162, 1999.

[4] E. Rodriguez, N. George, J. P. Lachaux, B. Renault, and F. J. Varela, "Perception's shadow: long-distance synchronization of human brain activity," *Nature*, vol. 397, pp. 430–433, 1999.

[5] A. Brovelli, M. Ding, A. Ledberg, Y. Chen, R. Nakamura, and S. L. Bressler, "Beta oscillations in a large-scale sensorimotor cortical network: Directional influences revealed by Granger causality," *Proc. Natl. Acad. Sci.*, vol. 101, pp. 9849–9854, 2003.

[6] G. Nolte, A. Ziehe, V. V. Nikulin, A. Schlögl, A. Krämer, T. Brismar, and K. R. Müller, "Robustly estimating the flow direction of information in complex physical systems," *Phys. Rev. Lett.*, vol. 100, p. 234101, 2008.

[7] A. V. Oppenheim and R. W. Schafer, *Discrete-Time Signal Processing*, 2nd ed. Englewood Cliffs, NJ: Prentice-Hall, 1999.

[8] V. V. Nikulin, K. Linkenkaer-Hansen, G. Nolte, S. Lemm, K. R. Müller, R. J. Ilmoniemi, and G. Curio, "A novel mechanism for evoked responses in the human brain," *Eur. J. Neurosci.*, vol. 25, pp. 3146–3154, 2007.

[9] M. L. Van Quyen, J. Foucher, J. P. Lachaux, E. Rodriguez, A. Lutz, J. Martinerie, and F. J. Varela, "Comparison of Hilbert transform and wavelet methods for the analysis of neuronal synchrony," *J. Neurosci. Methods*, vol. 11, pp. 83–98, 2001.

Ayumu Matani (M'96) received the B.E., M.E., and Ph.D. degrees in control engineering from Osaka University, Osaka, Japan, in 1989, 1991, and 1998, respectively.

From 1991 to 1995, he was with Osaka Gas Company Ltd., and with Nara Institute of Science and Technology during 1995 through 1998. He is currently an Associate Professor at the Graduate School of Frontier Sciences, the University of Tokyo, Kashiwa, Japan, and an invited Researcher with the Biological ICT Group, National Institute of Information and Communication Technology, Kobe, Japan. His research interests include signal processing, complex system theory, and brain imaging.

Yasushi Naruse received the B.E. degree in mathematical engineering and information physics from the University of Tokyo, Tokyo, Japan, and the M.S. and Ph.D. degrees in complexity science and engineering from the University of Tokyo, Kashiwa, Japan, in 2002, 2004, and 2007, respectively.

He is currently an Expert Researcher with the Biological ICT Group, National Institute of Information and Communication Technology, Kobe, Japan. His research interests include signal processing and modeling of neural activities.

Yasushi Terazono received the B.E. and M.E. degrees in mathematical engineering and information physics, and the Ph.D. degree in complexity science and engineering from the University of Tokyo, Tokyo, Japan, in 1999, 2001, and 2004, respectively.

From 2004 to 2009, he was with National Institute of Information and Communication Technology, Kobe, Japan. He is currently a Postdoctoral Fellow with the Graduate School of Frontier Sciences, the University of Tokyo, Kashiwa. His research interests include inverse problems and mathematical programming.

Taro Iwasaki received the B.E. degree in mechanical engineering from Tokyo University of Science, Tokyo, Japan in 2008. He is currently working toward the M.S. degree at the Graduate School of Frontier Sciences, the University of Tokyo, Kashiwa, Japan.

His current research interests include signal processing for complex biological systems.

Norio Fujimaki (M'80) received the B.E., M.E., and Ph.D. degrees in electronics engineering from the University of Tokyo, Tokyo, Japan, in 1975, 1977, and 1980, respectively.

From 1980 to 1999, he was with Fujitsu Laboratories Ltd., Atsugi, Japan. He is currently a Senior Researcher with the Biological ICT Group, National Institute of Information and Communication Laboratory, Kobe, Japan (since 1999), a Visiting Professor with the Graduate School of Life Science and Systems Engineering, Kyushu Institute of Technology, Kitakyushu, Japan (since 2001), and with the Human Information System Laboratories, Kanazawa Institute of Technology, Kanazawa, Ishikawa, Japan (since 2005). His research interest is measurements of linguistic brain functions.

Tsutomu Murata received the B.S., M.S., and Ph.D. degrees in pharmaceutical sciences (biophysics of the brain) from the University of Tokyo, Tokyo, Japan, in 1985, 1987, and 1993, respectively.

From 1992 to 1998, he was with Kanazawa Institute of Technology, Kanazawa, Ishikawa, Japan. He is currently the Subleader of Biological ICT Group, National Institute of Information and Communication Laboratory, Kobe, Japan. His research interests include psychophysics and neuroscience of emergent visual recognition.

Phase-Interpolated Averaging for Analyzing Electroencephalography and Magnetoencephalography Epochs

Ayumu Matani*, *Member, IEEE*, Yasushi Naruse, Yasushi Terazono, Norio Fujimaki, *Member, IEEE*, and Tsutomu Murata

***Abstract*—Stimulus-locked averages of electroencephalography (EEG) and magnetoencephalography (MEG) epochs reveal characteristic waveforms. EEG/MEG generation models to have reconstruct such waveforms have been recently proposed. These models assume that evoked, phase-modulated, and amplitude-modulated activities occur solely or simultaneously. We propose a two-stage stimulus-locked averaging method, called phase-interpolated averaging, to investigate the EEG/MEG generation process. First, virtual EEG/MEG epochs, which would be obtained as if instantaneous phases for each time sampling point were on a phase-grid, are interpolated from actually measured EEG/MEG epochs. Then, the virtual EEG/MEG epochs are discrete Fourier transformed. A simulation revealed that the zeroth Fourier term revealed the evoked activity, the first Fourier term revealed the amplitude-modulated activity, and the condition number of the interpolation reflected the phase-modulated activity. On the basis of these facts, a preliminary EEG analysis implied that the evoked activity is much smaller than what would be expected by using conventional averaging, the evoked and phase-modulated activities simultaneously occur, and the amplitude-modulated activity occasionally associates with the evoked and phase-modulated activities. To the best of our knowledge, this is the first time that these three activities have been shown to coexist by actually separating them.**

***Index Terms*—Amplitude modulation, averaging, electroencephalography (EEG), evoked activity, magnetoencephalography (MEG), phase modulation, phase reset.**

I. Introduction

STIMULUS-LOCKED averages (conventional averages, hereafter) of electroencephalography (EEG) and magnetoencephalography (MEG) epochs have characteristic waveforms called the contingent negative variation (CNV), visual potential/field, Go potential/field, and NoGo potential/field, etc. [9].

EEG/MEG (xEG, hereafter) generation models to reconstruct such waveforms have been recently studied. The simplest model is the evoked model. An evoked activity common to all xEG epochs is added to ongoing rhythmic activities just like an impulse response. Since the evoked activity is stimulus-locked and ongoing rhythmic activities contrarily are not so in this model, the conventional average will converge to the evoked activity. Thus, most researchers who perform conventional averaging, regardless of whether they do it explicitly or implicitly, adopt the evoked model.

The second model is the phase-reset model [1]. The phase reset is a sort of phase modulation; instantaneous phases jump to a specific phase as a result of stimuli, and thereby the distribution of the instantaneous phases changes from uniform to biased. The conventional average reveals the waveform caused by this bias. There has recently been a debate about which of these models is correct [6] and the possibility of both of them coexisting has been pointed out [7]. Phase modulation, and temporal- and spatial-phase synchronization/desynchronization in the brain have also been pointed out [2]–[4], which means that the conventional average contains biases that the phase-related phenomena produce. A hypothesis relating the phase synchronization/desynchronization to the phase reset has been proposed [5].

A third xEG generation model [8] has been proposed. In this model, the conventional average is the result of an amplitude modulation of a baseline-shifted ongoing rhythmic activity.

The aforementioned models are based on one or more elementary processes: evoked (EV), phase-modulated (PM), and amplitude-modulated (AM) activities. Therefore, in order to investigate the xEG generation process, these elementary processes should be separately extracted from measured xEG epochs. However, only the evoked activity is additive, and this means separating them is not a simple task. In this paper, we propose a stimulus-locked averaging method, called phase-interpolated averaging, for this purpose.

II. Method

We begin by outlining an interpretation of phase-compensated averaging [5] that will lead us to phase-interpolated averaging.

Manuscript received June 8, 2010; revised July 30, 2010; accepted September 20, 2010. Date of publication September 30, 2010; date of current version December 17, 2010. This work was supported in part by a Grant-in-Aid for Scientific Research (B) (No. 21300102) from the Ministry of Education, Science, Sports and Culture. *Asterisk indicates corresponding author.*

*A. Matani is with Graduate School of Frontier Sciences, The University of Tokyo, Kashiwa 277-8561, Japan, and also with Biological ICT Group, National Institute of Information and Communication Technology, Kobe 651-2492, Japan (e-mail: matani@isp.ac).

Y. Naruse and T. Murata are with Biological ICT Group, National Institute of Information and Communication Technology, Kobe 651-2492, Japan (e-mail: y_naruse@po.nict.go.jp; benmura@po.nict.go.jp).

Y. Terazono is with Graduate School of Frontier Sciences, the University of Tokyo, Kashiwa 277-8561, Japan (e-mail: teraz@isp.ac).

N. Fujimaki is with Biological ICT Group, National Institute of Information and Communication Technology, Kobe 651-2492, Japan, with Graduate School of Life Science and Systems Engineering, Kyushu Institute of Technology, Kitakyushu 808-0196, Japan, and also with the Human Information System Laboratories, Kanazawa Institute of Technology, Kanazawa 921-8501, Japan (e-mail: fujimaki@po.nict.go.jp).

Color versions of one or more of the figures in this paper are available online at http://ieeexplore.ieee.org.

Digital Object Identifier 10.1109/TBME.2010.2081990

Note that phase-interpolated averaging is not a modification of phase-compensated averaging, since it has a different purpose.

A. Phase-Compensated Averaging

Phase-compensated averaging has been proposed as a way of evaluating the directional relationship between xEG channels. The autoaverage of phase-compensated averaging is outlined as follows. The xEG time series of a channel, qth epoch ($q = 0, 1, \ldots, Q-1$), and nth time sampling point is denoted by $x_q[n]$ ($n = 0$: stimulus onset timing). First, $x_q[n]$ is narrow-band filtered (e.g., alpha–beta band) and Hilbert transformed to get $\tilde{x}_q^{\mathrm{N}}[n]$. Second, the instantaneous phase $\mathrm{Arg}\{\tilde{x}_q^{\mathrm{N}}[n_0]\}$ at the time sampling point n_0 is calculated. Third, $x_q[n]$ is wide-band filtered (e.g., delta–gamma band) and Hilbert transformed to get $\tilde{x}_q^{\mathrm{W}}[n]$. Finally, the autoaverage of phase-compensated averaging is determined as

$$\bar{x}^{n_0}[n] = \frac{1}{Q}\sum_{q=0}^{Q-1} \tilde{x}_q^{\mathrm{W}}[n] \exp\left(-\mathrm{j}\mathrm{Arg}\left\{\tilde{x}_q^{\mathrm{N}}[n_0]\right\}\right), \quad (1)$$

where j is the imaginary unit. Thus, the wideband xEG epochs $\tilde{x}_q^{\mathrm{W}}[n]$ are averaged with their narrow-band instantaneous phase $\mathrm{Arg}\{\tilde{x}_q^{\mathrm{N}}[n_0]\}$ compensated to be zero. The autoaverage (1) evaluates how the phase alignment of the xEG epochs at n_0 maintains or decays over time, and it implicitly includes the phase-preservation index [11]. One can find that the conventional average

$$\bar{x}[n] = \frac{1}{Q}\sum_{q=0}^{Q-1} x_q^{\mathrm{W}}[n] \quad (2)$$

is the autoaverage (1) in the case of $\mathrm{Arg}\{\tilde{x}_q^{\mathrm{N}}[n_0]\} = 0$.

Let us consider a virtual case:

$$\mathrm{Arg}\left\{\tilde{x}_q^{\mathrm{N}}[n_0]\right\} = \frac{2\pi q'}{Q}, \qquad (q' = 0, 1, \ldots, Q-1). \quad (3)$$

Equation (3) means that all of the instantaneous phases $\mathrm{Arg}\{\tilde{x}_q^{\mathrm{N}}[n_0]\}$ are on different phase-grids $2\pi q'/Q$, where the map $q \mapsto q'$ is one-to-one. Under the grid-phase sampling condition (3), or no jitter condition, the autoaverage (1) will be the first term of the discrete Fourier transform. Although the conventional average (2) is apparently the zeroth Fourier term without the grid-phase sampling condition (3), this condition is necessary in order to truly call the conventional average the zeroth Fourier term in contrast to the first Fourier term. Moreover, on the basis of this Fourier aspect, the phase-sorted xEG epoch order q', which is completely different from the stimulus presentation number q, can be given a physical meaning in the same way that "time" and "channel" have physical meanings.

B. Procedure of Phase-Interpolated Averaging

Phase-interpolated averaging separately extracts the EV, PM, and AM activities. It is extremely unlikely for measured xEG epochs to satisfy the grid-phase sampling condition (3), even at a time sampling point. Phase-interpolated averaging consists of two stages: I) virtual xEG epochs satisfying the grid-phase sampling condition (3) are estimated by interpolating measured xEG epochs and 2) the virtual xEG epochs are discrete Fourier transformed. Stage II seeks to remove only PM, whereas stage II seeks to separately extract EV and AM from the residual signal. Note that unlike phase-compensated averaging: 1) only the wide band xEG epochs are necessary and 2) stages I and II are done for each time sampling point and for each xEG channel (only auto term). Note that "wideband xEG" (in contrast to "narrow-band xEG") is actually limited to a small range of less than 40–50 Hz (mainly the alpha and delta bands), and the sampling frequency is usually set at several hundreds hertz or higher. Therefore, objective xEG epochs can be generally regarded as narrow-band limited.

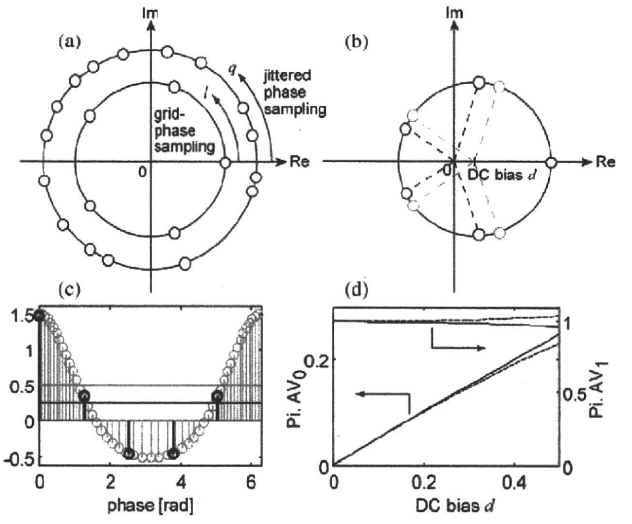

Fig. 1. Phase-interpolated averaging. (a) Concept of interpolation of phase sampling. Outer circle: Phase sampling. Instantaneous plots of measured xEG epochs having a constant amplitude on the complex plane can be treated as phase samples. Phase sampling always suffers from jitter. Inner circle: Virtual xEG epochs estimated by interpolating the measured xEG epochs. The interpolation resolves the phase-sampling jitters. (b) DC-bias problem of interpolation. Gray circles: Virtual xEG epochs estimated by interpolating about d. Black circles: Virtual xEG epochs estimated by interpolating about the axis origin. (c) Gray stems: Original 50-trial xEG epochs (dc bias $d = 0.5$) phase-sampled about the axis origin. Horizontal gray line: The mean of the original xEG epochs. Black stems: Virtual xEG epochs ($K = 2$). Horizontal black line: The mean of the virtual xEG epochs. (d) Zeroth and first phase-interpolated averages plotted versus dc bias d. These plots are used to compute multiplication coefficients η_0 and η_1.

1) Stage I (Interpolation): Fig. 1(a) shows the concept of interpolation. The outer circle illustrates instantaneous xEG epochs (complex-valued) on the complex plane; their amplitudes, or radii, are constant, for simplicity. Thus, this would be called phase sampling. Unlike time sampling, phase sampling is cropped from 0 to 2π and necessarily has a lot of sampling jitter; i.e., 2π is not equally divided. The inner circle illustrates phase sampling without jitter, namely grid-phase sampling.

The interpolation generates virtual xEG epochs satisfying the grid-phase sampling condition (3) from the measured xEG epochs on the basis of the periodic version of sampling theory, as follows. Let us consider phase sampling from continuous to discrete phases. The xEG time series of a channel, nth time sampling point, and continuous phase ψ is denoted by $x_n(\psi)$.

Since $x_n(\psi)$ is treated as periodic, $x_n(\psi)$ can be approximated by the partial sum up to $\pm K$th order of the Fourier series

$$x_n(\psi) \simeq \sum_{k=-K}^{K} c_n[k] \exp(\mathrm{j}k\psi), \tag{4}$$

where

$$c_n[k] = \frac{1}{2\pi} \int_{-\pi}^{\pi} x_n(\psi) \exp(-\mathrm{j}k\psi)\, \mathrm{d}\psi. \tag{5}$$

Note that $c_n[0]$ (dc amplitude) and $c_n[1]$ (fundamental-frequency amplitude) are the continuous Fourier transform versions of the conventional average at n and the autoaverage (1) at n, respectively. This indicates that these two terms, respectively, correspond to EV and AM (only fundamental term) without mutual leakage. If grid-phase sampling for $2K+1$ (from $-K$ to K) epochs is performed for $x_n(\psi)$, the discrete Fourier transform version of (5) is simply

$$c_n^{\mathrm{G}}[k] = \frac{1}{2K+1} \sum_{l=0}^{2K} x_n\left(\frac{2\pi l}{2K+1}\right) \exp\left(-\mathrm{j}\frac{2\pi kl}{2K+1}\right). \tag{6}$$

The superscript "G" stands for grid-phase sampling. Substituting (6) into (4), we get

$$\begin{aligned} & x_n(\psi) \\ & \simeq \sum_{k=-K}^{K} c_n^{\mathrm{G}}[k] \exp(\mathrm{j}k\psi) \\ & = \sum_{k=-K}^{K} \frac{1}{2K+1} \sum_{l=0}^{2K} x_n\left(\frac{2\pi l}{2K+1}\right) \exp\left(-\mathrm{j}\frac{2\pi kl}{2K+1}\right) \exp(\mathrm{j}k\psi) \\ & = \sum_{l=0}^{2K} x_n\left(\frac{2\pi l}{2K+1}\right) \frac{1}{2K+1} \sum_{k=-K}^{K} \exp\left(\mathrm{j}k\left(\psi - \frac{2\pi l}{2K+1}\right)\right) \\ & = \sum_{l=0}^{2K} x_n\left(\frac{2\pi l}{2K+1}\right) \mathrm{diric}_{2K+1}\left(\psi - \frac{2\pi l}{2K+1}\right), \end{aligned} \tag{7}$$

where

$$\mathrm{diric}_{2K+1}(\psi) = \frac{\sin((2K+1)\psi/2)}{(2K+1)\sin(\psi/2)} \tag{8}$$

is the Dirichlet kernel of the $2K+1$th order. Equation (7) corresponds to the periodical version of sampling theory.

Now, let us turn to the jittered sampling case, which is not so simple. By using the Fourier series (7), the phase-sorted q'th xEG epoch having phase-sampling jitters can be calculated as

$$\boldsymbol{x}_n^{\mathrm{J}} \simeq \boldsymbol{\Xi}_n \boldsymbol{x}_n^{\mathrm{G}}, \tag{9}$$

where

$$\begin{aligned} \boldsymbol{x}_n^{\mathrm{J}} &= [x_n(\psi_n^{\mathrm{J}}[0]) \cdots x_n(\psi_n^{\mathrm{J}}[q']) \cdots x_n(\psi_n^{\mathrm{J}}[Q-1])]^{\mathrm{T}}, \\ \boldsymbol{x}_n^{\mathrm{G}} &= \left[x_n(0) \cdots x_n\left(\frac{2\pi l}{2K+1}\right) \cdots x_n\left(\frac{2\pi K}{2K+1}\right)\right]^{\mathrm{T}}, \\ \boldsymbol{\Xi}_n &= [\xi_{xq'l}], \quad \xi_{xq'l} = \mathrm{diric}_{2K+1}\left(\psi_n^{\mathrm{J}}[q'] - \frac{2\pi l}{2K+1}\right). \end{aligned} \tag{10}$$

The superscript "J" stands for jittered phase sampling. Note that $\psi_n^{\mathrm{J}}[q']$ is calculated by using the epochwise discrete Hilbert transform; i.e., $\psi_n^{\mathrm{J}}[q']$ is only here treated as a function of n. See the Appendix for a discussion of the underdeterminedness of $\psi_n^{\mathrm{J}}[q']$.

By setting K such that $2K+1 < Q$, which means a reduction in the number of xEG epochs, we can estimate x_n^{G} in the least squares sense as

$$\hat{\boldsymbol{x}}_n^{\mathrm{G}} = \left[\boldsymbol{\Xi}_n^{\mathrm{T}} \boldsymbol{\Xi}_n + \lambda^2 \mathbf{I}_{2K+1}\right]^{-1} \boldsymbol{\Xi}_n^{\mathrm{T}} \boldsymbol{x}_n^{\mathrm{J}}, \tag{11}$$

where $\mathbf{I}_{2K+1}$ is the $2K+1$th unit matrix and λ^2 is a regularization parameter. Thus, we obtain the virtual xEG epoch $\hat{\boldsymbol{x}}_n^{\mathrm{G}}$. The condition number of $\boldsymbol{\Xi}_n$ in (10) indicates the difficulty of the interpolation, and therefore, it also qualitatively reflects PM. The optimal K (interpolation order) and λ^2 will be computed in Section III-E.

2) Stage II (Discrete Fourier Transform): Here, we are interested in only the zeroth and the real part of the first Fourier terms; the estimate of $c_n^{\mathrm{G}}[0]$ is called the zeroth phase-interpolated average and that of $2\mathrm{Re}\{c_n^{\mathrm{G}}[1]\} = c_n^{\mathrm{G}}[1] + c_n^{\mathrm{G}}[2K]$ is called the first phase-interpolated average. Stage II estimates $c_n^{\mathrm{G}}[0]$ and $2\mathrm{Re}\{c_n^{\mathrm{G}}[1]\}$ of (6) by taking the discrete Fourier transform of the virtual xEG epoch $\hat{\boldsymbol{x}}_n^{\mathrm{G}}$. The reason the first phase-interpolated average is not simply the estimate of $c_n^{\mathrm{G}}[1]$ is that $\hat{\boldsymbol{x}}_n^{\mathrm{G}}$ is real-valued. These two averages are, respectively, expressed as

$$\begin{aligned} \bar{x}_0[n] &= \frac{\eta_0}{2K+1} \sum_{l=0}^{2K} \hat{x}_n^{\mathrm{G}}\left(\frac{2\pi l}{2K+1}\right), \\ \bar{x}_1[n] &= \frac{\eta_1}{2K+1} \mathrm{Re}\left\{\sum_{l=0}^{2K} \hat{x}_n^{\mathrm{G}}\left(\frac{2\pi l}{2K+1}\right) \exp\left(-\mathrm{j}\frac{2\pi l}{2K+1}\right)\right\}, \end{aligned} \tag{12}$$

where η_0 and η_1 are the multiplier coefficients, which will be computed in Section II-C. Note that only $\bar{x}_0[n]$ and $\bar{x}_1[n]$ are objectives of interest at the moment, and therefore, a whole calculation of the discrete Fourier transform is not necessary.

C. Multiplier Coefficients η_0 and η_1

Since the zeroth and first phase-interpolated averages $\bar{x}_0[n]$ and $\bar{x}_1[n]$ of (12) are the estimates of $c_n^{\mathrm{G}}[0]$ and $2\mathrm{Re}\{c_n^{\mathrm{G}}[1]\}$ of (6), respectively, one may think that the multiplier coefficients η_0 and η_1 in (12) should be set to 1 and 2 accordingly. However, these values are correct, only if the instantaneous phases are calculated without a dc bias. This dc bias is what the evoked

model is about. Therefore, η_0 and η_1 are used for compensation of the dc bias.

Let us explain the dc bias problem and compute appropriate η_0 and η_1 in (12). Suppose that there is a continuous one-periodic sinusoid having unit amplitude with an unknown dc bias d and the original 50-trial xEG epochs are obtained by phase sampling the sinusoid under condition (3) about d; i.e., grid-phase sampling is performed with d as its center. The gray circles of Fig. 1(b) show virtual xEG epochs estimated by interpolating the original xEG epochs about d. The interpolation is almost identical to simple resampling in this case. The mean of the original xEG epochs is, of course, d, and that of the virtual xEG epochs is also d. Note that the situation up to this point is the same as in Fig. 1(a) because the dc bias does not affect the situation.

However, the actual interpolation is performed not about an unknown dc bias, but about the axis origin, as shown by the black circles in Fig. 1(b). The gray stems, i.e., the gray lines with circles, of Fig. 1(c) show the original xEG epochs phase-sampled about the axis origin (dc bias $d = 0.5$). Phase-sampling jitters occur, but the grid-phase sampling condition (3) will be satisfied if it is done about $d = 0.5$. The mean of the original xEG epochs, which is shown by the horizontal gray line, is still d. On the other hand, the black stems indicate the virtual xEG epochs ($K = 2$). The virtual xEG epochs seem to be properly placed as interpolations. However, the mean of the virtual xEG epochs, i.e., the horizontal black line, is not d because of the resolved phase-sampling jitters. Therefore, η_0 in (12) should not be set to 1. Similarly, η_1 should also be recomputed.

Fig. 1(d) shows the zeroth and first phase-interpolated average changes (stacked for $K = 1, 2, \ldots, 6$ in (6), tentatively, $\eta_0 = 1$ and $\eta_1 = 2$) versus d. Note that these averages, except those of $K = 1$ (dashed lines), overlap. Although there are slight differences with different K, the zeroth phase-interpolated averages are roughly $d/2$ and the first ones are roughly 1 independent of d. Therefore, $\eta_0 = 2$ and $\eta_1 = 2$ are employed accordingly.

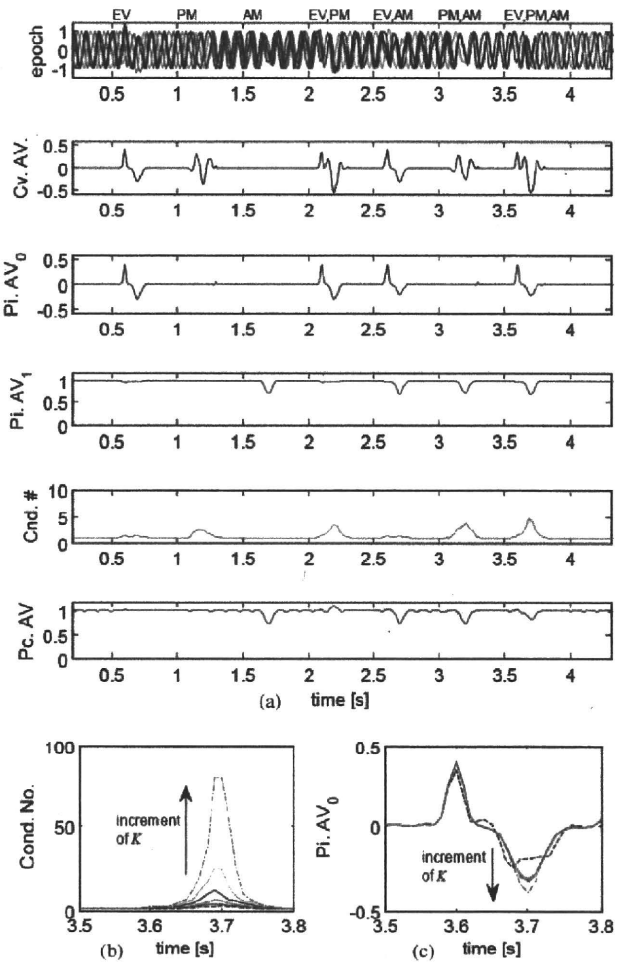

Fig. 2. Simulation of phase-interpolated averaging. (a) Top row: Five samples ($q = 0$, 10, 20, 30, and 40) of the given 50-trial xEG epochs. Second row: Conventional average. Third row: Zeroth phase-interpolated average ($K = 3$). Fourth row: First phase-interpolated average ($K = 3$). Fifth row: Condition number ($K = 3$). Bottom row: Phase-compensated average. (b) Change in condition number for a duration of 3.5–3.8 s with increment of $K = 1, 2, \ldots, 6$ (from bottom to top, broken lines: $K = 1, 6$). (c) Change in zeroth phase-interpolated average for a duration of 3.5–3.8 s with increment of $K = 1, 2, \ldots, 6$ (from top to bottom, broken lines: $K = 1, 6$). The simulation had a sampling frequency of 100 Hz.

III. Simulation

Phase-interpolated averaging is a means of investigating the xEG generation process. Even if three xEG activities (EV, AM, and PM) do not solely occur, phase-interpolated averaging should separate them as if each of them occurred solely. We performed a simulation to evaluate the separation ability of phase-interpolated averaging. Note that we did not have any prior hypothesis that these xEG activities occurred solely or simultaneously.

A. Given Epochs

Single-channel and 50-trial xEG epochs $x_q(t)$, $(q = 0, 1, \ldots, 49, 0 \le t \le 4.5\,\mathrm{s})$ were given as

$$x_q(t) = x^{\mathrm{EV}}(t) + a^{\mathrm{AM}}(t)\cos\theta_q^{\mathrm{PM}}(t), \tag{13}$$

where $x^{\mathrm{EV}}(t)$ was the EV, $a^{\mathrm{AM}}(t)$ was the AM, and $\theta_q^{\mathrm{PM}}(t)$ was the epoch-wise PM. Note that AM and PM are not simply superimposed. The top row of Fig. 2(a) shows five samples of $x_q(t)$. EV, PM, and AM solely or simultaneously occurred in durations of $t \in [0.5u,\ 0.5u + 0.3]$, $(u = 1, 2, \ldots, 7)$. EV, PM, and AM were set as follows.

EV consisted of two Gaussian functions

$$x^{\mathrm{EV}}(t) = \begin{cases} 0.4\exp(-5\cdot 10^3(t-(0.5u+0.1))^2) \\ \quad -0.3\exp(-10^3(t-(0.5u+0.2))^2), & u = 1,4,5,7 \\ 0, & \text{otherwise.} \end{cases} \tag{14}$$

PM consisted of random phase connections [5]

$$\theta_q^{\mathrm{PM}}(t) = \begin{cases} \psi_{q(u-1)}(t), & 0.5u \le t \le 0.1 + 0.5u \\ \begin{pmatrix} \psi_{qu}(0.3 + 0.5u) \\ -\psi_{q(u-1)}(0.1 + 0.5u) \end{pmatrix} \cdot \left(\dfrac{t - 0.1 + 0.5u}{0.2}\right) & 0.1 + 0.5u < t \le 0.3 + 0.5u \\ \quad + \psi_{q(u-1)}(0.1 + 0.5u), & \\ \psi_{qu}(t), & 0.3 + 0.5u < t < 0.5u, \end{cases} \tag{15}$$

where

$$\psi_{qu}(t) = \begin{cases} 2\pi \cdot 10t + \dfrac{2\pi P_u[q]}{50}, & u = 2, 4, 6, 7 \\ 2\pi \cdot 10t + \dfrac{2\pi P_{u-1}[q]}{50}, & \text{otherwise} \end{cases} \tag{16}$$

and $P_u[q]$ denotes the random permutation of the integer numbers from 0 to 49 for the uth duration and $P_0[q] = q$.

AM consisted of a Gaussian envelope:

$$a^{\mathrm{AM}}(t) = \begin{cases} 1 - 0.3\exp(-10^3(t - (0.2 + 0.5u))^2), & u = 3, 5, 6, 7 \\ 1, & \text{otherwise.} \end{cases} \tag{17}$$

If the baseline shift and amplitude modulation model [8] is taken into account, (13) should be modified into

$$\begin{aligned} x_q'(t) &= a'^{\mathrm{AM}}(t)\left(x^{\mathrm{EV}}(t) + \cos\theta_q^{\mathrm{PM}}(t)\right) \\ &= a'^{\mathrm{AM}}(t)x^{\mathrm{EV}}(t) + a'^{\mathrm{AM}}(t)\cos\theta_q^{\mathrm{PM}}(t). \end{aligned} \tag{18}$$

Therefore, this model is already included in (13) when EV is also amplitude-modulated.

B. Conventional Averages

The second row of Fig. 2(a) shows the conventional average. EV and PM each generated activity, and the EV activity was superimposed on the PM activity when they simultaneously occurred. Thus, when the conventional average is not zero, it is impossible to identify which of only EV, only PM, or both EV and PM occurred.

C. Phase-Interpolated Averages

Phase-interpolated averaging was performed for $K = 3$. The third row of Fig. 2(a) shows the zeroth phase-interpolated average. Even if EV occurs with PM and/or AM, the zeroth phase-interpolated average quantitatively extracted only EV. The fourth row of Fig. 2(a) shows the first phase-interpolated average. The first phase-interpolated average quantitatively extracted the envelope of only AM. The fifth row of Fig. 2(a) shows the condition number of Ξ_n in (10). It qualitatively reflected the biased distributions of the instantaneous phases caused by only PM. Therefore, we can say that phase-interpolated averaging successfully separated EV, PM, and AM.

Let us briefly compare phase-interpolated averaging and conventional time-series analyses, such as the complex wavelet transform and Hilbert transform. One may think that the absolute values of the complex wavelet transform and the Hilbert transform of an xEG epoch can be used to estimate AM. However, these transforms produce nonzero activity even in the EV-only case: $x_q(t) = x^{\mathrm{EV}}(t)$, and thereby, they cannot separate EV and AM.

D. Phase-Compensated Averages

The bottom row of Fig. 2(a) shows the phase-compensated average in which xEG epochs (13) were used for both the narrow- and wideband xEGs. Although phase-compensated averaging has no notion of the zeroth and first averages, let it suffice here to say that the zeroth and first averages, respectively, correspond to the conventional [because of (2) and (12)] and incomplete first phase-interpolated (in the meaning that phase-compensated averaging led to the phase-interpolated average in Sections II-A and II-B) averages.

The zeroth phase-compensated average shows PM-contaminated EV. The first phase-compensated average showed EV–PM-contaminated AM (e.g., 2.1–2.3 s). Moreover, phase-compensated averaging is not able to detect PM separately. Therefore, the interpolation, which is the main difference between phase-compensated and phase-interpolated averaging, is necessary for the separation. Note that the purpose of phase-compensated averaging is not separation, but rather analysis of cross-channel directional synchronization.

E. Optimal Interpolation Order K and Regularization Parameter λ^2

Theoretically speaking, the larger the K is, the more accurate the interpolation will be. However, a much larger K should also make the condition number of the interpolation much larger. A very large K would thus degrade the accuracy of the interpolation. The reason the accuracy of the interpolation depends on K because the Fourier series (7) with interpolation (11) is not an orthogonal expansion.

Let us compute the optimal K and the regularization parameter λ^2. Fig. 2(b) shows the condition numbers for $K = 1, 2, \ldots, 6$ for a duration of 3.5–3.8 s for which EV, PM, and AM simultaneously occurred in the simulation. As expected, the condition number increased with the increment of K. Fig. 2(c) shows the zeroth phase-interpolated averages ($K = 1, 2, \ldots, 6$). They mostly overlapped for $K = 2, 3, \ldots, 5$, and EV was robustly and accurately reconstructed as (14) in this range of K. Fig. 2(b) and (c) roughly indicates that the upper bound of the condition number κ^{sup} for yielding an upper bound of K for accurate interpolation is about 20 or 30.

κ^{sup} can also help us to set λ^2 in (11). Note that λ^2 is only for stabilizing the pseudo inverse of Ξ_n. Too much stabilization degrades the accuracy of the interpolation to the extent that EV and PM cannot be separated. Thus, λ^2 should be set less than $(s^{\max}/\kappa^{\mathrm{sup}})^2$, where $s^{\max}$ is the maximum singular value of Ξ_n.

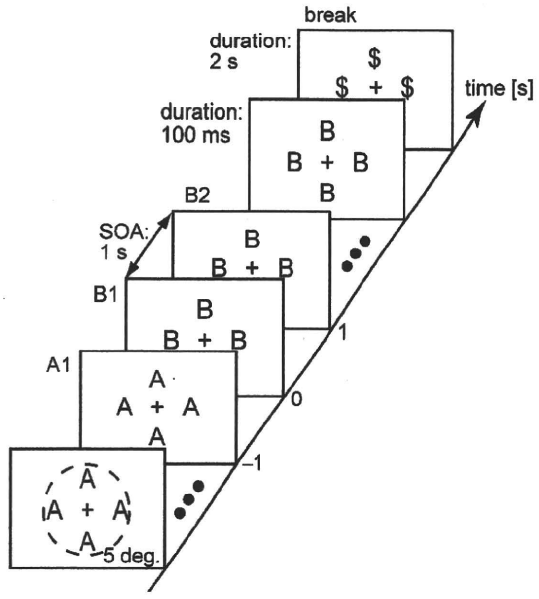

Fig. 3. Schematic diagram of the button-pressing experiment. 320 stimulus sequences, each of which consisted of A-images first, then B-images, and finally a $-image (eight images in total), was presented (40 sequences × 8 runs). The total number of A- and B-images was 7, and the number of A-images randomly changed from 1 to 5. Each image consisted of four A, B, or $ characters surrounding the fixation point + within 5° of visual angle. Each of the A- or B-images was displayed for 100 ms, and the stimulus onset asynchrony (SOA) was 1 s. The $-image was displayed at the end of every stimulus sequence for a 2-s break (e.g., for blinking). Subjects were instructed to press a button as soon as they saw the first B-image (B1).

For instance, $\kappa^{\sup}$ indicates that $(s^{\max}/100)^2$ would be a better choice for λ^2, and this is the value we employed.

In practice, phase-interpolated averaging should be performed for several Ks by referencing the changes in the condition number and ensuring the robustness of the averaging results.

IV. Results and Discussion

The good simulation results encouraged us to conduct phase-interpolated averaging on experimentally measured EEG epochs.

A. EEG Recording

Six subjects (Subjects 1–6) participated in a button-pressing experiment during which EEG recordings were made. Fig. 3 shows a schematic diagram of the experiment. The subjects were instructed to look at 320 stimulus sequences, each of which consisted of eight serially presented images (A-images, then B-images, and finally a $-image), and to press a button immediately when they saw the first B-image, which appeared with an unknown timing. In the stimulus sequences, the first B-image was symbolically called "B1" (onset: 0 s), the second B-image was called "B2" (onset: 1 s), and the A-image just preceding B1 was called "A1" (onset: −1 s). Thirty-one channels of EEG (extended international 10–20 system) were simultaneously recorded during the experiment (sampling frequency: 600 Hz). The reason we performed such a complex experiment was that we expected various potentials, e.g., visual (V), CNV, NoGo, and Go, to be included in the EEG epochs for A1, B1, and B2. Note that we excluded the EEG epochs where A1 was the first presented image in the stimulus sequences from further analysis for the reason explained in Section IV-B.

As preprocessing, EEG epochs having artifacts (e.g., blinking) in the duration to be analyzed and mistakes for button-pressing were eliminated and the remaining EEG epochs were bandpass filtered (with a finite impulse response filter: 1–50 Hz, 240th order). The valid EEG epochs numbered 251, 254, 252, 267, 269, and 261 for Subjects 1–6, respectively. The scope of this paper is not to discuss brain functions, but to describe a new averaging method and to investigate EEG generation processes. Hence, it is enough for our purpose to present an analysis of two-channel EEG (FC_z: located at frontal point on the medial line, O_z: located at the occipital point on the medial line).

The subjects gave written informed consent after they were given a detailed explanation of this study. The study received approval from the Ethics Committee for Human and Animal Research, Graduate School of Frontier Sciences, the University of Tokyo.

B. Conventional Averages

The thick gray lines in the top rows of Fig. 4(a) (FC_z) and (b) (O_z) show the conventional averages of Subject 1. The A1, B1, and B2 onsets are indicated on the horizontal axes. V potentials were observed for A1, B1, and B2 at FC_z and O_z for a duration of 100–250 ms after the stimulus onset. These V potentials could be simply caused by individual visual stimuli. CNV potentials were observed for A1 and B1 at FC_z in the pretrigger duration. These CNV potentials could be caused by the subject expecting the first B-image's appearance. In fact, a CNV potential was not observed for B2. The reason we excluded some of the EEG epochs prior to the analysis was that subjects did not seem to generate CNV for the first A-images, which were necessarily presented before the others. A NoGo potential was observed for A1 at FC_z for a duration of 200–500 ms after the stimulus onset. No NoGo potential was observed for B2, for which button-pressing was not necessary. A Go potential was observed for B1 at FC_z and also a part of that was observed at O_z for a duration of 200–500 ms after the stimulus onset. All of these potentials partially overlapped and may have included other event-related potentials, e.g., an attention-related one.

Subjects 2–6 showed very similar conventional averages. Table I summarizes the conventional averages of Subjects 1–6. The number of "+"s and the number in parentheses indicate a somewhat subjective amplitude of the activity and how many subjects showed such activity, respectively.

C. Phase-Interpolated Averages

The lines, except the thick gray ones, in Fig. 4 show the phase-interpolated averaging results of Subject 1. Fig. 4(c) (FC_z) and (d) (O_z) are the magnified views of Fig. 4(a) (FC_z) and (b) (O_z), respectively. The thin dashed, thin solid, and thin dash-dotted

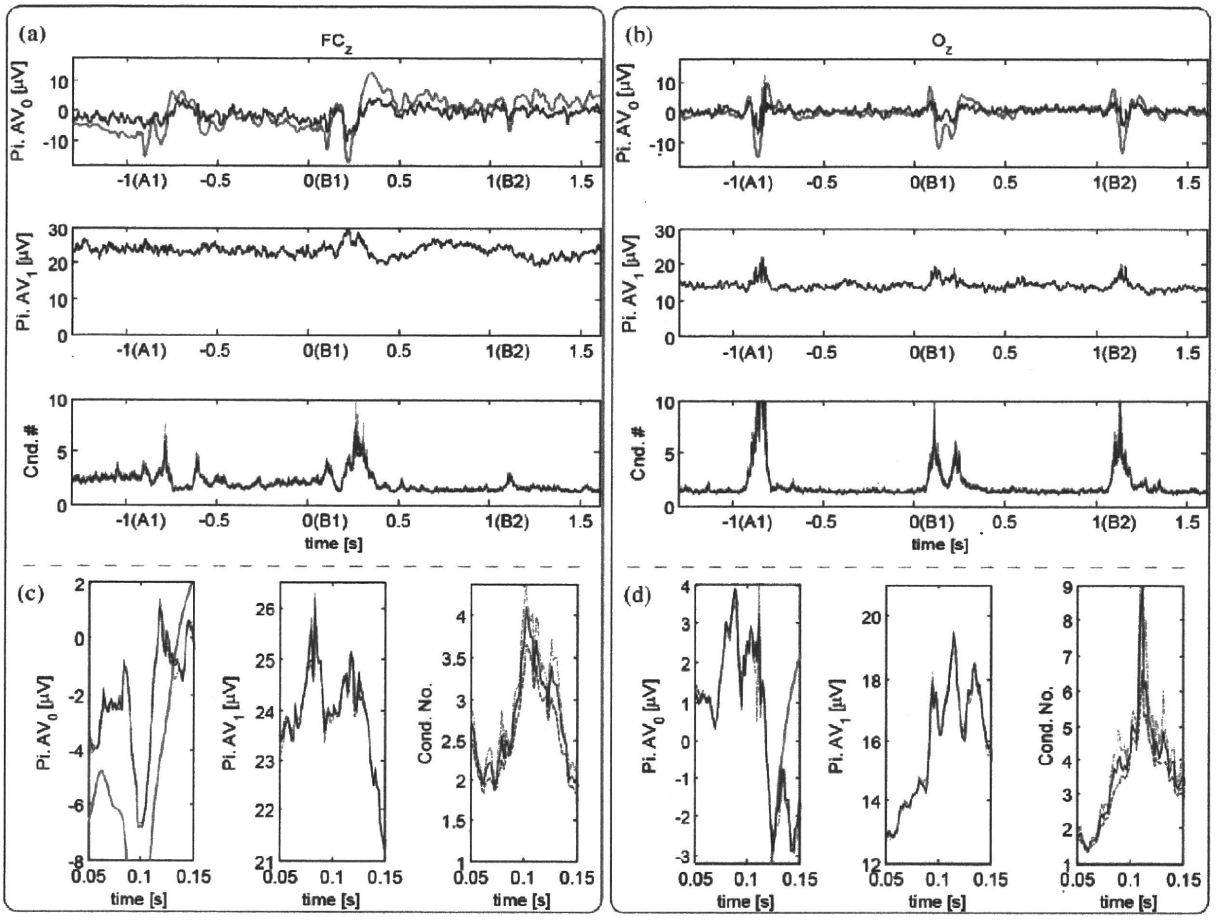

Fig. 4. Phase-interpolated averaging results of recorded EEGs [(a) and (c): FC_z; (b) and (d): O_z). Top rows of (a) and (b) Thick gray lines: conventional averages. Thin lines: zeroth phase-interpolated averages. Middle rows of (a) and (b) First phase-interpolated averages. Bottom rows of (a) and (b) Condition numbers. (c) and (d) Magnified views of (a) and (b) (0.05–0.15 s). Although the thin dashed, thin solid, and thin dash-dotted lines correspond to results for $K = 3$, 4, and 5, respectively, in all the plots, they mostly overlap, especially the zeroth and first phase-interpolated averages.

TABLE I
CONVENTIONAL AVERAGES OF SUBJECTS 1–6

electrode	duration	V	CNV	NoGo	Go
FCz	A1	++(6)	++(6)	++(5)	
	B1	++(5)	++(6)		+++(6)
	B2	++(5)			
Oz	A1	+++(5)		+(3)	
	B1	+++(5)			++(5)
	B2	+++(5)			

TABLE II
ZEROTH PHASE-INTERPOLATED AVERAGES OF SUBJECTS 1–6

electrode	duration	V	CNV	NoGo	Go
FCz	A1	+(4)	+(5)	+(5)	
	B1	+(5)	+(5)		++(5)
	B2	+(4)			
Oz	A1	++(3)			
	B1	++(4)			+(2)
	B2	++(3)			

lines correspond to results for $K = 3$, 4, and 5, respectively. The top, middle, and bottom rows of Fig. 4(a) and (b) correspond to the zeroth phase-interpolated averages, the first phase-interpolated averages, and the condition numbers of the interpolation, respectively. The zeroth and first phase-interpolated averages (three textured lines) mostly overlapped for the range of K, although a spiky disturbance was only seen for $K = 5$ in the left panel of Fig. 4(d). Thus, the overlapped phase-interpolated averages were somewhat reliable because they were similar to the simulation results [Fig. 2(c)].

The zeroth phase-interpolated averages showed 1) V potentials for A1, B1, and B2 at FC_z and O_z; 2) CNV potentials for A1 and B1 at FC_z; 3) a NoGo potential for A1 at FC_z; and 4) a Go potential for B1 at FC_z and also a part of that at O_z. All of the zeroth phase-interpolated averages were very similar to the conventional averages. However, their amplitudes were smaller than those of the conventional averages. The first phase-interpolated averages at O_z increased in the durations in which the V potentials were observed, and those at FC_z increased in the durations in which the Go potential was observed. The condition numbers at FC_z and O_z increased in the durations in which the V, part of NoGo, and Go potentials were observed.

Tables II–IV summarize the zeroth phase-interpolated averages, the first phase-interpolated averages, and the condition

TABLE III
FIRST PHASE-INTERPOLATED AVERAGES OF SUBJECTS 1–6

electrode	duration	V	CNV	NoGo	Go
FCz	A1				
	B1	+(1)			+(3)
	B2				
Oz	A1	+(5)			
	B1	+(5)			+(1)
	B2	+(4)			

TABLE IV
CONDITION NUMBERS OF SUBJECTS 1–6

electrode	duration	V	CNV	NoGo	Go
FCz	A1	+(6)	+(5)	++(5)	
	B1	+(6)	+(5)		++(6)
	B2	+(6)			
Oz	A1	++(6)		+(3)	
	B1	++(6)			++(6)
	B2	++(6)			

numbers of the interpolation, respectively, of Subjects 1–6. These presentation styles are the same as used for Table I.

D. EEG Generation Process

Let us briefly discuss the EEG generation characteristics common to the six subjects as a preliminary result. Tables I and II reveal that EV activities are smaller, occasionally vanishingly smaller, than the values estimated by using conventional averaging, but they highly probably exist. Tables II and IV indicate that EV and PM activities probably occur simultaneously and their ratio would vary as the case may be. The results in Tables II–IV suggest that AM activities occasionally associate with EV and PM activities and might modify the EV and PM activities. Consequently, the aforementioned aspects can be summed up that EV and PM models (including the phase reset model) coexist and the AM model (including the baseline shift and amplitude modulation model) occasionally occurs.

Finally, we should also consider that xEG-detectable activities in a single epoch are caused by the amount of the spatial synchronization of a huge number of neurons. The spatial synchronization in a single epoch might be a factor preventing us from making an unequivocal decision about the xEG generation process. The spatial synchronization in a single epoch would have EV-, AM-, and/or PM-like characteristics. Phase-interpolated averaging can investigate the spatial synchronization in a single epoch by substituting each neural activity for an xEG epoch; however, there is no method to measure tens of thousands of individual neurons noninvasively.

V. CONCLUSION

We presented a two-stage averaging method for xEG epochs, called phase-interpolated averaging, to separately investigate EV, PM, and AM activities. The first stage is the interpolation of xEG epochs as if grid-phase sampling were possible, and the second stage is a discrete Fourier transform of the interpolated xEG epochs. Phase-interpolated averaging separately extracts EV as the zeroth Fourier term, separately extracts the envelope of AM as the real part of the first Fourier term, and separately evaluates PM as the condition number of the interpolation. The results of a simulation and an EEG experiment using this method implied that 1) EV is much smaller than what would be with conventional averaging; 2) EV and PM activities simultaneously occur; and 3) AM activity occasionally associates with EV and PM activities. To the best of our knowledge, this is the first time that the coexistence of these three activities has been confirmed by actually separating them.

APPENDIX
UNDERDETERMINEDNESS OF INSTANTANEOUS PHASE GENERATION

Let us denote the discrete Fourier transform (DFT) and its inverse (DFT^{-1}) by using lower- and uppercases as follows:

$$X[k] = \mathrm{DFT}\{x[n]\},$$
$$x[n] = \mathrm{DFT}^{-1}\{X[k]\}, (n, k = 0, 1, \ldots, N-1). \quad \text{(A1)}$$

Complex-valued sequence $\tilde{x}[n]$ generation from a real-valued sequence $x[n]$ is based on at least the following two constraints. The first constraint is $x[n]$ and the real part of $\tilde{x}[n]$ are the same

$$x[n] = \mathrm{Re}\{\tilde{x}[n]\}. \quad \text{(A2)}$$

The second constraint is that they satisfy the symmetry relationships of the discrete Fourier transform

$$\begin{aligned}
\mathrm{DFT}\{\mathrm{ReEv}\{\tilde{x}[n]\}\} &= \mathrm{ReEv}\{\tilde{X}[k]\},\\
\mathrm{DFT}\{\mathrm{ReOd}\{\tilde{x}[n]\}\} &= \mathrm{ImOd}\{\tilde{X}[k]\},\\
\mathrm{DFT}\{\mathrm{ImEv}\{\tilde{x}[n]\}\} &= \mathrm{ImEv}\{\tilde{X}[k]\},\\
\mathrm{DFT}\{\mathrm{ImOd}\{\tilde{x}[n]\}\} &= \mathrm{ReOd}\{\tilde{X}[k]\}, \quad \text{(A3)}
\end{aligned}$$

where Re, Im, Ev, and Od stand for the real, imaginary, even function, and odd function parts, respectively. For instance, $\mathrm{ReEv}\{\cdot\}$ means the real and even function part of the sequence in the parenthesis. $\tilde{x}[n]$ and $\tilde{X}[n]$ in the top two rows of (A3) can be replaced with $x[n]$ and $X[n]$, because of (A2). Since there is no information for the bottom two rows of (A3), complex-valued signal generation requires an additional constraint. The discrete Hilbert transform generates the analytic sequence:

$$\tilde{x}[n] = \mathrm{DFT}^{-1}\{X[k]\, F[k]\}, \quad \text{(A4)}$$

in which the constraint is expressed as

$$F[k] = \begin{cases} 1, & k = 0, \dfrac{N}{2} \\ 2, & k = 1, 2, \ldots, \dfrac{N}{2} - 1 \\ 0, & k = \dfrac{N}{2} + 1, \dfrac{N}{2} + 2, \ldots, N-1 \end{cases} \quad \text{(A5)}$$

and N is an even number, for simplicity [10], [12]. $F[k]$ makes the negative frequency terms, which are actually thevadjust last

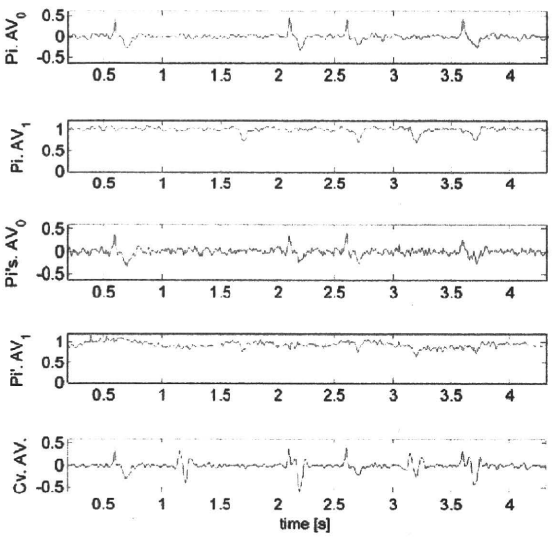

Fig. 5. Influence of the underterminedness of the discrete Hilbert transform on phase-interpolated averaging with noise. Top two rows: Zeroth and first phase-interpolated averages with the normal discrete Hilbert transform (with $F[k]$). Middle two rows: Zeroth and first phase-interpolated averages with an alternative discrete Hilbert transform (with $F'[k]$). Bottom row: Conventional average.

half of $X[k]$, zero. $F[k]$ also conserves the polarity-independent power spectrum

$$|X[k]|^2 + |X[N-k]|^2 = |\tilde{X}[k]|^2 + |\tilde{X}[N-k]|^2, \quad \left(k = 1, \ldots, \frac{N}{2} - 1\right). \quad \text{(A6)}$$

To satisfy (A2) and (A6), $F'[k]$ exists as an alternative to $F[k]$. $F'[k]$ treats negative frequency terms differently. One can swap 2 and 0 between $F[k]$ and $F[N-k]$; e.g., when $F[k]$ is [1 2 2 2 1 0 0 0], $F'[k]$, such as [1 0 2 2 1 0 0 2] and [1 2 0 0 1 2 2 0], can be used instead. In general, there are a total of $2^{N/2-1}$ variations.

Equation (A4) for each variation of $F'[k]$ generates a different $\mathrm{Im}\{\tilde{x}[n]\}$ and the same $\mathrm{Re}\{\tilde{x}[n]\}$. The $\tilde{x}[n]$s associated with $F'[k]$s are distributed on the horizontal line (A2) on the complex plane (symmetry about the real axis). $|\tilde{x}[n]|$ and $\mathrm{Arg}\{\tilde{x}[n]\}$ are thus underdetermined. In particular, if $X[k]$ is wideband, the distribution is accordingly wide. The phase interpolation based on $\mathrm{Arg}\{\tilde{x}[n]\}$ (11) is affected by this underdeterminedness. A different criterion must be necessary to deal with the underdeterminedness.

The first and second rows of Fig. 5 show the zeroth and first phase-interpolated averages with $F[k]$ for the simulated xEG epoch (13) with Gaussian noise (mean: 0, standard deviation: 0.25) added to widen the frequency band. The third and fourth rows show the phase-interpolated averages with an example of $F'[k]$ (randomly generated). The bottom row shows the conventional average. Although the phase-interpolated averages with $F[k]$ had a noise level similar to that of the conventional average, those with $F'[k]$ suffered from additional low- and high-frequency noise. Such additional noise, especially high-frequency noise, was observed even in the noise-free case and/or with a different $F'[k]$. Therefore, $F[k]$ is appropriate for phase-interpolated averaging.

$F[k]$ has another useful characteristic. Equation (A3) indicates that $\mathrm{DFT}^{-1}\{\mathrm{Od}\{F[k]\}\}$ is the periodic convolution kernel to produce $\mathrm{Im}\{\tilde{x}[n]\}$. $\mathrm{Od}\{F[k]\}$ (e.g., [0 1 1 1 0 −1 −1 −1]) is the longest bipolar pulse as an odd discrete finite-length sequence. Therefore, the time localization of $F[k]$ (e.g., $\mathrm{DFT}^{-1}\{[0\ 1\ 1\ 1\ 0\ -1\ -1\ -1]\}$) is not wider than that of any $F'[k]$. Consequently, the instantaneous phase associated with $F[k]$ is well time-localized.

Because of the aforementioned characteristics, $F[k]$ is sufficient for phase-interpolated averaging. Although some $F'[k]$ may work as well as $F[k]$, there is no good way to find such an $F'[k]$ among such huge variations.

REFERENCES

[1] S. Makeig, M. Westerfield, T. P. Jung, S. Enghoff, J. Townsend, E. Courchesne, and T. J. Sejnowski, "Dynamic brain sources of visual evoked responses," *Science*, vol. 295, pp. 690–694, 2002.

[2] Y. Naruse, A. Matani, T. Hayakawa, and N. Fujimaki, "Influence of seamlessness between pre- and post stimulus alpha rhythms on visual evoked potential," *NeuroImage*, vol. 32, pp. 1221–1225, 2006.

[3] C. Tallon-Baudry and O. Bertrand, "Oscillatory gamma activity in humans and its role in object representation," *Trends Cogn. Sci.*, vol. 3, pp. 151–162, 1999.

[4] E. Rodriguez, N. George, J. P. Lachaux, B. Renault, and F. J. Varela, "Perception's shadow: Long-distance synchronization of human brain activity," *Nature*, vol. 397, pp. 430–433, 1999.

[5] A. Matani, Y. Naruse, Y. Terazono, T. Iwasaki, N. Fujimaki, and T. Murata, "Phase-compensated averaging for analyzing electroencephalography and magnetoencephalography Epochs," *IEEE Trans. Biomed. Eng.*, vol. 57, no. 5, pp. 1117–1123, May 2010.

[6] P. Sauseng, W. Klimesch, W. R. Gruber, S. Hanslmayr, R. Freunberger, and M. Doppelmayr, "Are event-related potential components generated by phase resetting of brain oscillations? A critical discussion," *Neuroscience*, vol. 146, pp. 1435–1444, 2007.

[7] B. K. Min, N. A. Busch, S. Debener, C. Kranczioch, S. Hanslmayr, A. K. Engel, and C. H. Herrmann, "The best of both worlds: phase-reset of human EEG alpha activity and additive power contribute to ERP generation," *Intl. J. Psychophysiol.*, vol. 65, pp. 58–68, 2007.

[8] V. V. Nikulin, K. Linkenkaer-Hansen, G. Nolte, S. Lemm, K. R. Müller, R. J. Ilmoniemi, and G. Curio, "A novel mechanism for evoked responses in the human brain," *Eur. J. of Neurosci.*, vol. 25, pp. 3146–3154, 2007.

[9] E. Niedermeyer and F. L. da Silva, *Electroencephalography*, 5th ed. Baltimore, MD: Lippincott Williams and Wilkens, 2005.

[10] A. V. Oppenheim and R. W. Schafer, *Discrete-time Signal Processing*, 2nd ed. Upper Saddle River, NJ: Prentice Hall, 1999.

[11] A. Mazaheri and O. Jensen, "Posterior α activity is not phase-reset by visual stimuli," *Proc. Natl. Acad. Sci. USA*, vol. 103, pp. 2948–2952, 2006.

[12] B. Boashash, "Estimating and interpreting the instantaneous frequency of a signal–Part 1: Fundamentals," *Proc. IEEE*, vol. 80, no. 4, pp. 520–538, Apr. 1992.

Ayumu Matani (M'96) received the B.E., M.E., and Ph.D. degrees in control engineering from Osaka University, Osaka, Japan, in 1989, 1991, and 1998, respectively.

From 1991 to 1995, he was with Osaka Gas Company Ltd. From 1995 to 1998, he was with Nara Institute of Science and Technology. He is currently an Associate Professor at Graduate School of Frontier Sciences, the University of Tokyo, Kashiwa, Japan, and an Invited Researcher at Biological Information and Communication Technology (ICT) Group, National Institute of Information and Communication Technology, Kobe, Japan. His research interests include signal processing, complex system theory, and brain imaging.